Mon. Not. R. astr. Soc. (1992) **255**, 521–538

The APM Proper Motion Project – I. High proper motion stars

Dafydd Wyn Evans*
Institute of Astronomy, Madingley Road, Cambridge CB3 0HA

Accepted 1991 November 4. Received 1991 November 1; in original form 1990 April 11

SUMMARY

Results are presented on a subset of proper motion data with $|\mu| \gtrsim 0.04$ arcsec yr^{-1} from the APM Proper Motion Project. Comparisons made with the NLTT catalogue show that the levels of contamination and incompleteness in this catalogue are consistent with the random measuring errors in the proper motions. No significant zero-point offset is found in the NLTT proper motions with respect to that defined by galaxies. Reduced proper motions in the four fields studied are found to be very effective in distinguishing between various stellar populations when combined with colour information. The kinematic properties of these populations are investigated. From the white dwarf sample, a luminosity function is derived and is in very good agreement with that of Liebert, Dahn & Monet.

1 INTRODUCTION

In this paper the properties of the high proper motion stars measured in the APM Proper Motion Project will be discussed. For this work high proper motion stars are defined as those having $|\mu| \gtrsim 0.04$ arcsec yr^{-1}. The details concerning the proper motion measurements and the removal of the systematic errors present in the data is described in Evans (1988). The plate material used and the photometric calibration details are given in Evans (1989).

High proper motion selection has been a useful tool for astronomers since the early days of photographic astronomy. By blinking two plates by eye it was relatively easy to spot those objects with high motions. These were either nearby objects or those with intrinsically high motions, both of which were of interest to astronomy. This technique enabled a subset of interesting objects to be selected from the large number of objects on a plate, without having to measure all of them.

The most comprehensive high proper motion catalogue constructed is the NLTT catalogue (Luyten 1979). The contamination and completeness of this catalogue are discussed along with the random errors.

Various kinematic properties of the high proper motion (HPM) stars are considered. Estimates of the direction of solar motion are made for various population groups for all four fields. The possibility of using reduced proper motion (RPM) diagrams of HPM stars to classify them into population groups is discussed, along with the information that can be extracted from these diagrams.

Using RPM classifications a sample of white dwarfs is constructed. A luminosity function for these objects is estimated using the Schmidt (1975) $1/V_{\max}$ method. This was in preference to the method given in Chołoniewski (1987) due to the easier implementation of the $1/V_{\max}$ method.

2 CONTAMINATION OF THE HPM SAMPLE BY SPURIOUS OBJECTS

The HPM samples in each field comprise the stars with a proper motion greater than about 0.04 arcsec yr^{-1}. The proper motions are calculated by simply dividing the change in position of a star between the primary- and secondary-epoch plates by the time difference between the two epochs. Each plate is scanned twice. The second time the plate is rotated by 180°. This eliminates certain systematic errors that might arise due to the measuring process. The positions are then the average for the 0° and 180° scans of each plate. The primary-epoch plates are the red Palomar (E) plates, while the secondary ones are the United Kingdom Schmidt Telescope (UKST) J plates. The exception to this is the 8 Hour Field, in which the primary-epoch plate is the blue Palomar plate (O62). The reason for this is that the red plate, E62, has larger (unexplained) positional errors than normal.

* Present address: Royal Greenwich Observatory, Madingley Road, Cambridge CB3 0EZ.

Table 1. The positions of the four fields used in the project.

Name	RA		dec		l	b
	h	m	°	′	°	°
8 Hour Field	8	53	17	30	210	35
11 Hour Field	11	12	-20	00	274	37
12 Hour Field	12	05	11	30	268	71
15 Hour Field	15	00	0	00	357	48

Table 2. The proper motion limits, in arcsec per year, of the HPM samples considered in this chapter for all four fields of the project.

	Low proper motion limit	High proper motion limit
8 Hour Field	0.035	0.347
11 Hour Field	0.049	0.485
12 Hour Field	0.040	0.396
15 Hour Field	0.047	0.469

The secondary-epoch plate for the 8 Hour Field is J6814. The positions of the four fields are given in Table 1. For more details and a full list of plates see Evans (1989).

The actual lower limit chosen was a 16μ (~ 1 arcsec) change in position. This limit, combined with the upper position-change limit of 160μ (~ 10 arcsec) caused by restrictions within the matching algorithm (Evans 1988), implies slightly different proper motion limits for each field. These are given in Table 2. The size of the limit chosen is somewhat arbitrary, as is the case with all HPM samples. The main criteria were that the limit was large enough so that there would be no contamination due to the random error distribution (easily the case) and that the sample in each field would be around 2000, a manageable number.

The major problem with any sample of objects selected by their extreme parameters, e.g. HPMs, is contamination by spurious images. Although the fraction of images on a plate which have corrupted parameters is small, they will (usually) have their parameters changed from average values to extreme ones and will populate a region of parameter space

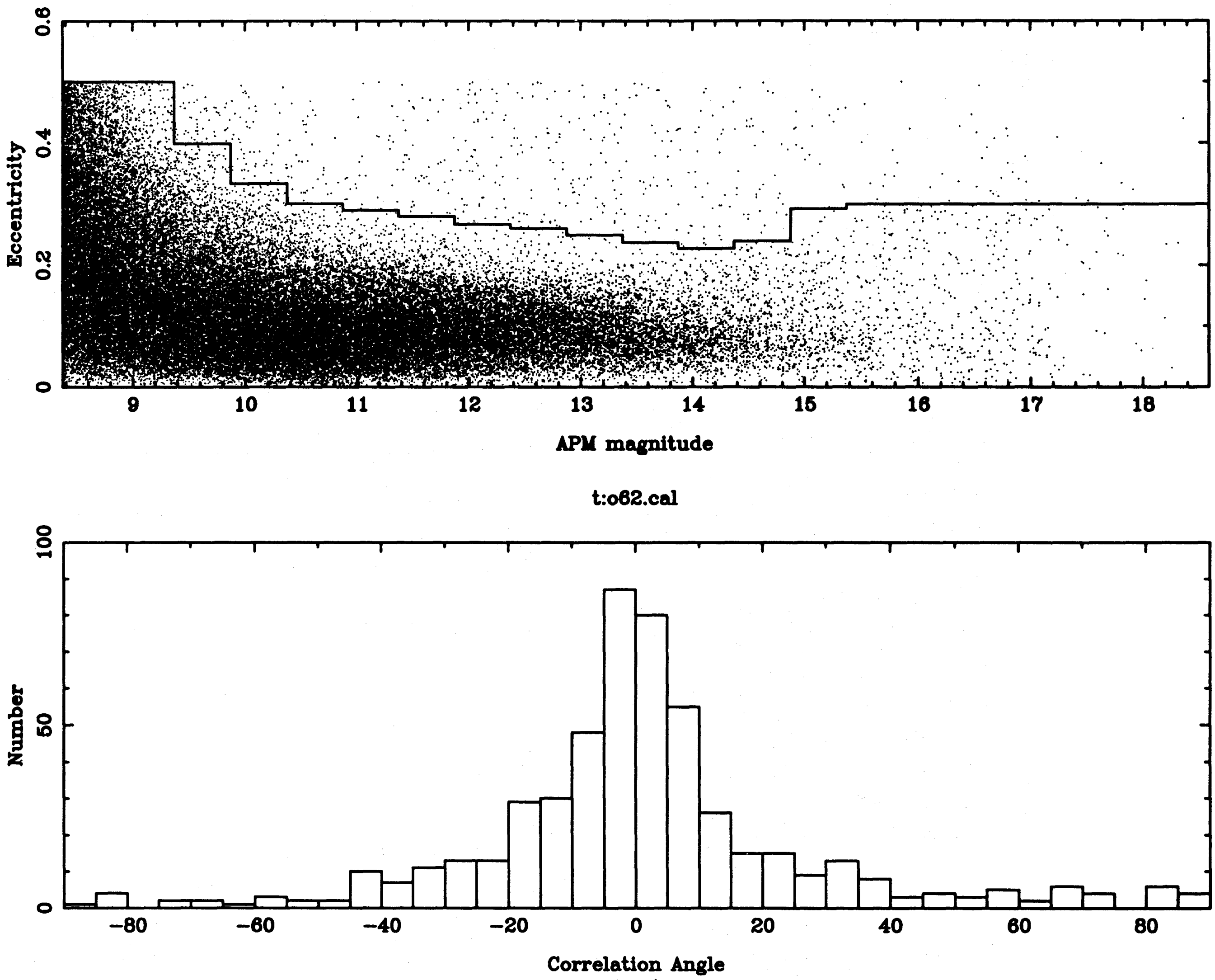

Figure 1. The top half shows a scatterplot of eccentricity versus APM magnitude ($=2.5\log_{10} I_{iso}$) for the stars on plate O62. The magnitude range in O is from 21 to 9 (the faint images are on the left). Note that no object is classified as a star if its eccentricity is above 0.5. The lines drawn are the eccentricity limits used to reject possible merged objects from the HPM sample. The bottom half shows the difference in angle between the orientation of an eccentric image's ellipse and its proper motion direction.

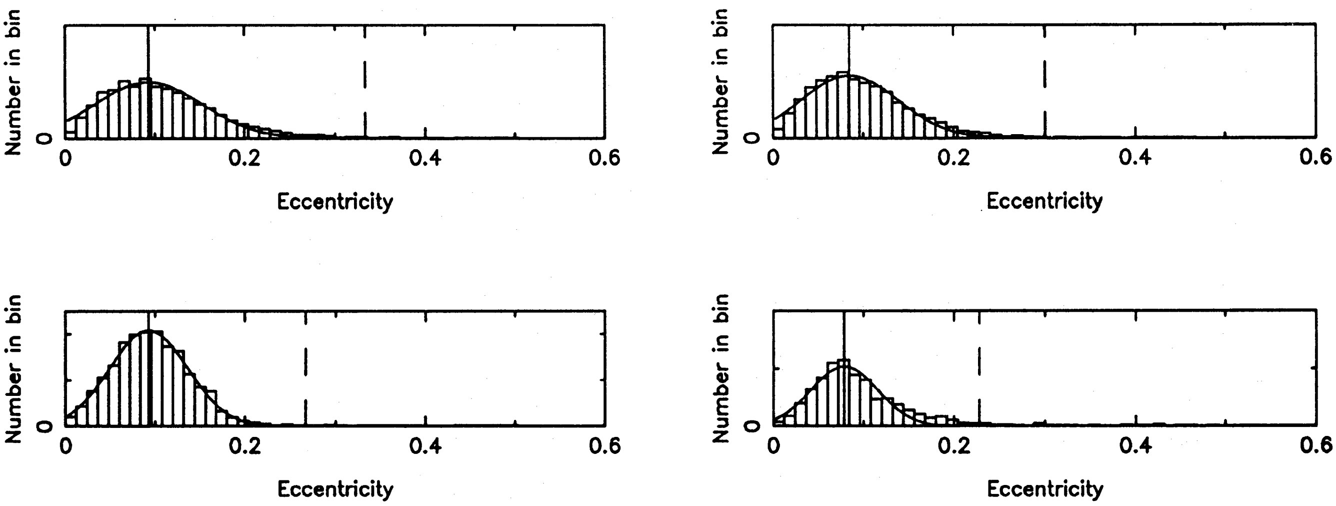

Figure 2. Examples of the eccentricity distribution in various magnitude bins for stars on O62, along with the Gaussian fit used to determine the eccentricity limit (dashed line). The approximate magnitudes for each bin are 18, 17.5, 15.5 and 13 mag.

where objects are normally scarce, becoming a significant contaminant.

One method used to remove these objects is to reject images with shapes which are more eccentric than normal. The images picked up in this way are mainly merged images, with a few bright stars which have an asymmetric image structure. The eccentricity (calculated using the second-order moments of the image) limits are a function of APM magnitude ($=2.5 \log_{10} I_{iso}$) and are determined from scatter-plots of eccentricity versus APM magnitude. An example is given in Fig. 1. The data are binned in half-magnitude intervals and a Gaussian is fitted to the eccentricity distribution within each bin. Although the distribution is not strictly speaking a Gaussian one, the procedure provides a robust estimate of the half-width. The limit is set at the mode of the distribution plus 4 half-widths. Fig. 2 shows four examples of the eccentricity distribution and corresponding Gaussian fits. The bottom diagram of Fig. 1 shows the correlation, for eccentric images, between the orientation angle of the image's ellipse (again calculated using the second-order moments of the image) and the direction of the apparent proper motion. This diagram shows how much a star's spurious proper motion is affected by having an image merge with another object.

Between 10 and 40 per cent of objects in each initial HPM sample are flagged as having an eccentric image on at least one plate. A full breakdown is given in Table 3. As a check on this classification procedure, 168 eccentric images were visually inspected on the plate O62. Of these, 135 (80 per cent) were merged objects, and six (4 per cent) had asymmetric image structures which would affect their proper motions. The remaining 27 (16 per cent) appeared as single stellar images. These classifications were of objects brighter than $O=20$ mag. 36 images were inspected which were fainter than this, but no reliable classification could be carried out for these objects. The reason for this is that the classification of an object as a merged image is not entirely straightforward. For faint images, the absence of a detected image could be due either to having merged with an adjacent image or by being below the detection limit set for the scanner.

Even for the brighter images, there can be some doubt as to how much any merging will affect the proper motion of the image. For example, if the images are merged on both of the plates which determine the proper motion, the systematic shift in proper motion will not be as large as if the merging had occurred on only one plate. Even so, the proper motion will still be in error, unless both stars have the same colour, since the photocentres will be different on the two plates. Therefore when rejecting merged objects, it must be realized that the remaining sample will be incomplete to some extent.

The second method used to remove spurious images is to reject those images which have positions which are different by more than ~1 arcsec on the O and E plates, which have no epoch difference between them. Any observed 'proper motion' for an image between these plates will be spurious and the image should therefore be rejected. This technique will pick up mismatches as well as merged images. Table 3 gives the number of objects in each field that were flagged by the two methods.

Again, as an estimate of the accuracy of the technique, a random sample of 204 moved images were visually inspected on plate O62. From this sample 111 (54 per cent) were merged images and 16 (8 per cent) were defective images of some other kind, e.g. a mismatch. The remaining 77 (38 per cent) appeared as single stellar images. Nevertheless, the scan positions of these objects are inconsistent between the O and E plates. Assuming that the spurious position change is due to a scanning error on only one of the plates and that the errors are divided evenly between the plates, only half of these objects should be rejected. Therefore the failure rate of the second rejection method is 19 per cent.

Table 3. The total number of objects with proper motions between the two limits quoted in Table 2 for each field. The number of spurious HPM images, found by the two methods mentioned in the text, is also given.

	Unflagged	Eccentric	Moved	Both
8 Hour Field	2167	334	147	341
11 Hour Field	1014	298	19	169
12 Hour Field	2497	189	68	129
15 Hour Field	1018	391	135	326

Table 4. The results of a visual inspection of 202 randomly selected HPM images in the 8 Hour Field. The Flagged category includes images rejected by either or both of the rejection methods outlined in the text.

	True	Possibly False	False
Unflagged	136 (67%)	22 (11%)	2 (1%)
Flagged	10 (5%)	10 (5%)	22 (11%)

To check the overall completeness and contamination, a random sample of 202 HPM objects was selected from those in the 8 Hour Field and visually inspected on plate O62. In addition to the True (no problems with the image) and False (a defective image, e.g. two stellar images merging) HPM Image categories, a Possibly False category was also used. This was due to the uncertainty in classifying some merged images which has been mentioned previously. The results of these classifications are given in Table 4. The two extreme interpretations of the Possibly False category yield the following values for contamination (C) and incompleteness (I) in the HPM sample. If they are all False images, $C=18$ and $I=7$ per cent and if all True, $C=1$ and $I=11$ per cent.

Another method for estimating incompleteness and contamination uses the distribution of the proper motion directions (θ) for the Flagged (as a spurious image by the analysis programs) and Unflagged images. For this incompleteness estimate, two assumptions are made: (i) False images have a flat θ distribution; (ii) the θ distribution of the Flagged True images will have the same shape as the Unflagged True images. In other words, these assumptions are that neither the processes creating False images, nor the rejection methods, have a preferred direction. If the shape of the Unflagged distribution is linearly transformed to fit the shape of the Flagged distribution, the incompleteness of the Unflagged sample can be calculated from $I=g/(1+g)$, where g is the gradient of the linear transformation used. The results of this method are given in Table 5. The errors quoted are calculated using the errors in measuring g. Using the θ distribution only a maximum contamination estimate can be made. Again, the assumption that False images have a flat θ distribution has been made. The estimate is made by setting the amount of contamination of a flat θ distribution to be equal to the lowest level of the Unflagged distribution. The lowest level is determined by taking the average of the five lowest bins in the distribution. This level is the maximum that a flat distribution could contaminate the sample. Naturally, the contamination could be much lower, since the True-image θ distribution could easily have a flat part to it. The maximum contamination in each field is given in Table 5. No error estimates are given since this is only a maximum contamination limit.

Table 5. The incompleteness and maximum contamination of the HPM samples for all four fields using the θ distributions.

	Maximum Contamination	Incompleteness
8 Hour Field	8.0%	9.5(±1.5)%
11 Hour Field	10.7%	10.4(±1.6)%
12 Hour Field	2.9%	7.2(±0.7)%
15 Hour Field	12.9%	18.1(±2.4)%

As an example, Fig. 3 shows the Flagged and Unflagged θ distributions for the 15 Hour Field. This field has the *highest* values for maximum contamination and incompleteness.

Considering the failure rates of 16 and 19 per cent for the two rejection methods and the numbers in each category from Table 3, the following incompleteness values $I_8=8.5$, $I_{11}=9.8$, $I_{12}=3.4$ and $I_{15}=16.6$ per cent are obtained. These values agree quite well with the values given in Table 5, especially considering that the failure rates could be in error by 3 per cent.

In summary, the incompleteness of the HPM samples due to the rejection methods is around 9 per cent except in the

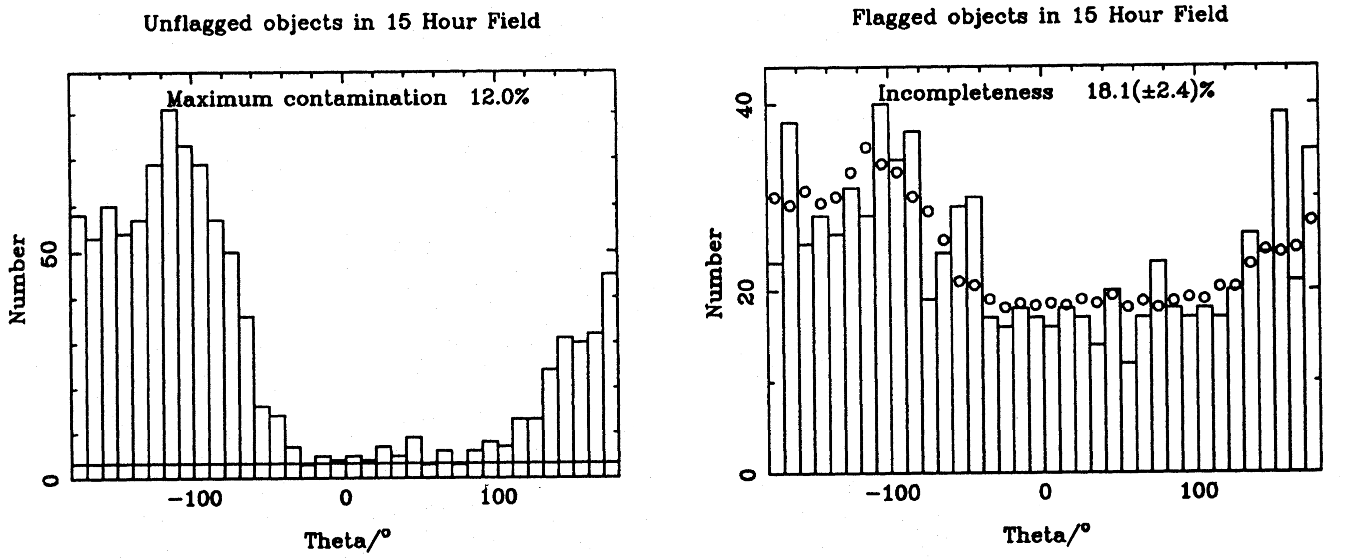

Figure 3. The proper motion direction, θ, distribution for Unflagged (first panel) and Flagged (second panel) images. In the first panel the maximum contamination level by False images is made by setting it equal to the lowest level of the distribution (solid line near bottom). The second panel shows the θ distribution of the Flagged images (histogram) with the linearly transformed Unflagged θ distribution plotted as circles. From the gradient of this linear transformation, the incompleteness is calculated.

15 Hour Field where it is about twice this value. In addition to this, there will be an extra incompleteness of ~9 per cent due to stars being misclassified as galaxies (see Evans 1988). The maximum contamination varies from field to field but is lower than 13 per cent.

3 COMPARISON WITH LUYTEN'S NLTT CATALOGUE

General catalogues of stars with large proper motions have been around since the turn of the century. The early catalogues, such as Porter (1892) and van Maanen (1915), had proper motions which were generally determined from meridian circle observations. The situation progressed rapidly with the advent of photographic surveys and the use of blink comparators. The first large-scale survey was the Bruce Proper Motion Survey, using the Bruce Telescope in South Africa, and was completed in 1937. From this two high proper motion catalogues were published, the LHS (Luyten Half Second) catalogue (Luyten 1955) and the LTT (Luyten Two Tenths) catalogue (Luyten 1957, 1961, 1962). Both of these catalogues were periodically updated. A similar proper motion survey was carried out by the Lowell Observatory (Giclas, Burnham & Thomas 1971).

The biggest problem with these catalogues was that since the search had to be carried out by eye, using a blink comparator, there would be observer bias and a possible large incompleteness present. This difficulty was overcome with use of an automated–computerized scanner and measuring machine, described in La Bonte (1970) and Newcomb (1975), to locate and measure the HPM stars on the plates taken for the Palomar Proper Motion Survey. The final catalogue, known as the NLTT catalogue (Luyten 1979), had a lower proper motion limit of 0.18 arcsec yr^{-1} and a limiting blue magnitude of ~21. This limiting magnitude was only applicable to declinations north of $-33°$, where plates from the regular Palomar Survey were available. South of $-33°$ plates from the Bruce Survey were used and have blue limits of between 15.5 and 17.5 mag. Regions of low galactic latitude were excluded from the survey due to the difficulties of measuring proper motions in crowded fields.

Table 6. The counting statistics of the comparison made between the NLTT catalogue and this project's HPM sample. The first column gives the number of stars in each field that are in both samples. The number in parentheses is the number of stars in this category with $\mu<0.18$ arcsec yr^{-1}. The second column gives the number of NLTT stars which were rejected from the HPM sample by either or both of the methods described in Section 2. Column 3 gives the number of NLTT stars that were not included in the original HPM sample (usually due to misclassification as galaxies). The fourth column gives the number of NLTT stars which cannot be identified or had spuriously high proper motions. The last column gives the number of stars in the HPM sample with $\mu>0.18$ arcsec yr^{-1} which were not in the NLTT catalogue. All objects in the last three columns have been visually inspected.

	Unflagged	Flagged	NLTT star missed	Incorrect NLTT star	$\mu > 0''.18$/y not in NLTT
8 Hour Field	21 (2)	2	4	2	7
11 Hour Field	21 (3)	2	1	–	3
12 Hour Field	50 (18)	5	3	3	12
15 Hour Field	19 (—)	2	1	–	3

The comparison presented here with the NLTT catalogue goes as faint as $O\sim21$ mag, since none of the four fields are at low galactic latitude and all are north of declination $-33°$. Considering the boundary limits of the fields, the proper motion limits of Table 2 and a bright limit of $E=11$ mag, 136 Luyten NLTT stars should be included in this project's HPM sample (four NLTT stars were not considered, since they were fainter than the intensity cut-offs used in each field). The numbers of NLTT stars found by this project, as well as the number of objects with $\mu>0.18$ arcsec yr^{-1} missed by Luyten are given in Table 6.

The ratio of flagged to unflagged NLTT objects agrees very well with the estimate of 9 per cent for the incompleteness in the HPM sample due to the rejection methods being incorrect. The other NLTT objects not in the HPM sample (column 3 of Table 6) are due to errors in the star/galaxy separation algorithm and one mismatch. These numbers are consistent with the number of stars misclassified as galaxies given in Evans (1988). The fourth column gives the number of stars which should not be included in the comparisons. The two stars in the 8 Hour Field indicated in this column cannot be found at the positions stated and no other image is present within an arcminute. The usual accuracy of the NLTT positions is 0.1 arcmin. The stars from this column in the 12 Hour Field have incorrect proper motions given in the NLTT catalogue. The measured proper motions are all less than 0.04 arcsec yr^{-1} (*cf.* NLTT limit of 0.18 arcsec yr^{-1}) and should not be included in the comparison.

The last column gives the number of stars in this project's HPM sample with $\mu>0.18$ arcsec yr^{-1} that were not included in the NLTT catalogue. These objects have a range of magnitudes of $21>O>14$. The low numbers of objects available make it difficult to estimate the true proper motion direction distributions of these stars. However, the observed distributions are similar to those of Fig. 3. The observed total proper motion distributions show about two-thirds of stars with proper motions in the range $0.18<\mu_{\rm total}<0.20$ arcsec yr^{-1}. If these stars had spuriously high proper motions, the vast majority ($\gtrsim 90$ per cent) would have proper motions in the range $0.20<\mu_{\rm total}\lesssim 0.45$ arcsec yr^{-1}. It is quite probable that most of these stars have been left out of the NLTT catalogue, due to measuring errors causing the measured proper motion to fall below the 0.18 arcsec yr^{-1} limit. Similarly, this will account for some of the NLTT stars which have proper motions from this project of less than 0.18 arcsec yr^{-1} (numbers in parentheses in first column of Table 6). A Monte Carlo simulation carried out to predict these numbers produced the following results. For the contamination numbers, $n_8=4$, $n_{11}=6$, $n_{12}=19$ and $n_{15}=1$. For the numbers of stars missed by Luyten, $n_8=5$, $n_{11}=1$, $n_{12}=8$ and $n_{15}=2$. The large number of objects contaminating the NLTT sample for the 12 Hour Field is due to the slightly larger NLTT proper motion errors for this field.

As can be seen, the predicted contamination numbers are close to the observed values, indicating that the contamination can be explained by random measuring errors in the NLTT catalogue. Similarly, the predicted numbers of missed stars are about the same as the observed numbers, showing that random measuring errors can explain approximately all the incompleteness in the NLTT catalogue.

Summarizing, there is between 10 and 20 per cent contamination in the NLTT catalogue which is probably due

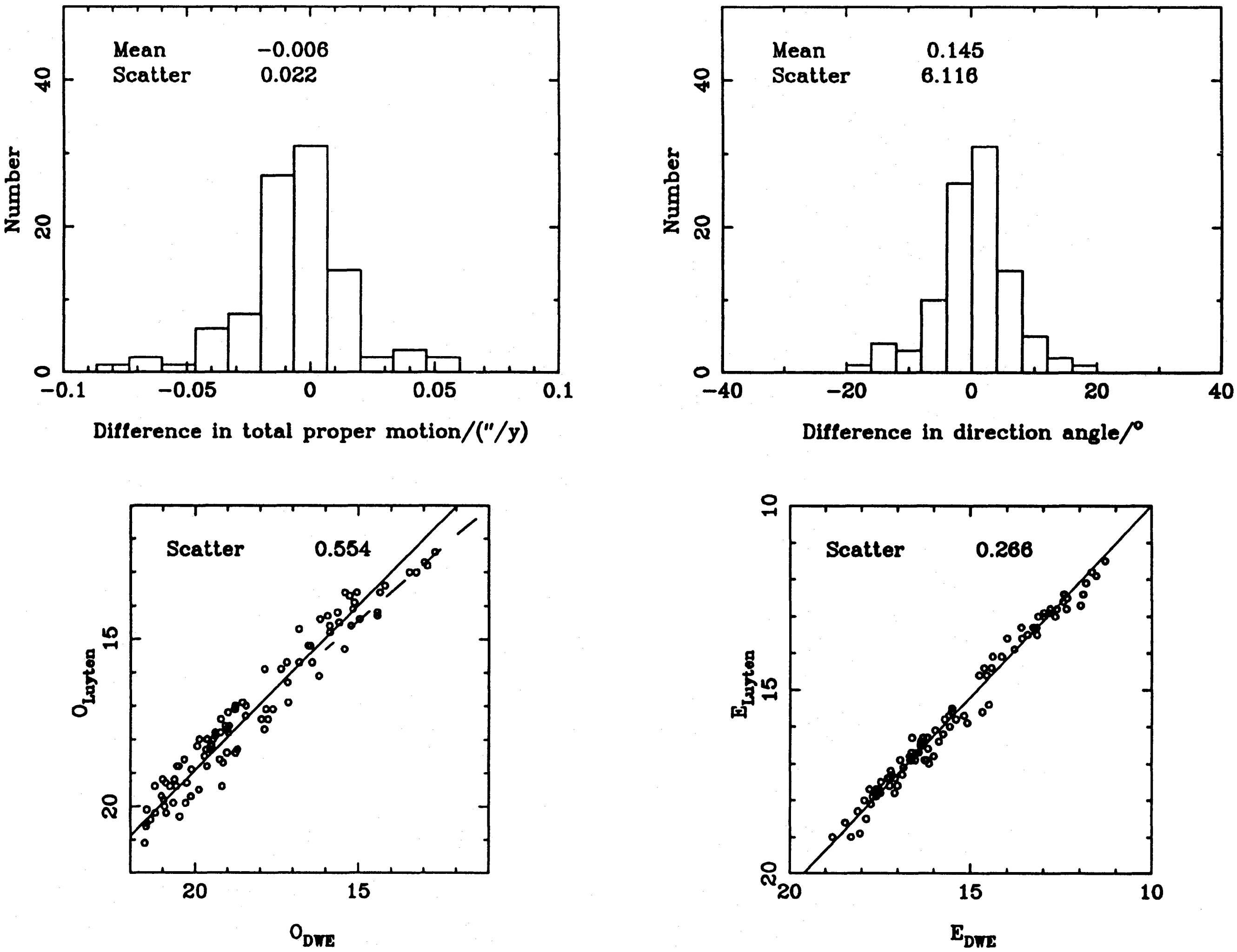

Figure 4. A comparison between proper motion and photometry values found in the NLTT catalogue and this project's HPM sample (all four fields). The top two panels show the differences (my value minus NLTT value) in proper motion size and direction. The bottom two panels show the photometric comparison. The solid lines are least-squares linear fits to the data and the quoted scatter values are the rms scatter of the NLTT values about these lines. The dashed line drawn in the third panel is the correction calculated by Gliese & Jahreiß (1980) to convert from the NLTT blue estimates to *B*.

entirely to random measuring errors. There is also about 16 per cent incompleteness, again, probably due entirely to random errors in the measuring of the proper motions.

The errors in the astrometry and photometry are presented in Fig. 4. Since the errors from this project are around 0.005 arcsec yr^{-1} and 0.09 mag (Evans 1988) the differences presented in the comparison are almost all due to the errors in the NLTT catalogue.

The rms of the distributions of the differences in total proper motion and proper motion direction, using the data from all fields, are 0.022 arcsec yr^{-1} and 6.1° respectively. These values are consistent with each other and agree with the error estimate given in Luyten (1979). For each field, the total proper motion error deduced from the difference distributions ranges from 0.014 arcsec yr^{-1} (8 Hour Field) to 0.027 arcsec yr^{-1} (12 Hour Field). When the proper motions were measured for the NLTT catalogue, relative values were obtained which were then corrected to absolute values. The maximum value for these corrections was 0.016 arcsec yr^{-1}. By considering the errors in the proper motion components (μ_α and μ_δ, the proper motion components in the direction of increasing right ascension and declination) it is possible to see if these corrections have been applied correctly, since the proper motions measured from this project are absolute ones due to using galaxies to define an astrometric reference frame. Considering the low numbers of objects in each field it is only possible to measure the mean of the proper motion error to an accuracy of about 0.005 arcsec yr^{-1}. In only one case out of eight does the measured mean exceed this value (μ_δ in the 8 Hour Field) where the mean is 0.010 arcsec yr^{-1}. These means are consistent with the corrections to absolute motions having been applied correctly in the NLTT to within 0.005 arcsec yr^{-1}.

The scatter of the photometric differences measured using the data from all fields is 0.55 mag for *O* and 0.27 mag for *E*. These values are the scatter about the best-fit linear relation between the NLTT photometry and that from this project. For both passbands the gradient of this relation is close to 1, but while the zero-point difference between the two sets of measurements for the *E* magnitudes is zero, there is about a magnitude difference for the *O* measurements, i.e. $O_{NLTT} \approx O_{DWE} - 1$. The reason for this difference is that the

NLTT blue values are all estimates determined by eye (Luyten 1968). A systematic correction as a function of magnitude has been measured by Gliese & Jahreiß (1980) down to about $O \approx 16$ mag and this has been drawn as the dashed line in Fig. 4. As can be seen, these corrections are consistent with the data. Since these corrections are strictly only applicable to the B passband (and not O) there may be a difference of ~ 0.2 mag.

The NLTT red calibrations were carried out by comparing a deep photoelectric sequence in field SA57 (North Galactic Pole) with the image diameters of the stars on the corresponding Palomar plates. This calibration was then used in all other fields of the survey. Variation in the photographic conditions will cause shifts in the zero-point of the magnitude system. Therefore some of the scatter seen in Fig. 4 is due to this. The average rms calculated from each field is 0.44 mag for O and 0.17 mag for E. The value for the E passband agrees with the estimate given in La Bonte (1970) of the scatter from the SA57 calibration. The difference given in Gliese & Jahreiß (1980) of ~ 0.8 mag between Luyten's red magnitudes and those of Eggen (1979) for red stars, is probably due to the differences between the E and R_K (Kron, Gascoigne & White 1957) passbands.

4 THE KINEMATIC PROPERTIES OF THE HPM SAMPLE

One of the main problems in analysing the kinematic properties of a sample of stars arises when two or more populations, with possibly different kinematics, are present. Even if the kinematics are very different (greater than a factor of 2 difference), it is often still difficult to extract information out of solely proper motion data, since there is considerable overlap in the proper motion values of the different populations. In these cases, considerable weight is given to the wings of the distributions (where there is hardly any overlap) and here it is extremely important to have accounted for all the non-Gaussian errors in the data. Naturally, if the kinematic properties of the different populations are similar, more information is required to distinguish between them.

4.1 Reduced proper motions

A useful way of combining proper motions with photometric data is the parameter H, the reduced proper motion (RPM). Reduced proper motion was first used by Hertzsprung and later extended by Luyten (1922) and is the proper motion equivalent to absolute magnitude. It is defined by

$$H = m + 5\log_{10}\mu + 5$$
$$= M + 5\log_{10} T - 3.379, \qquad (1)$$

where m is the apparent magnitude, μ the total proper motion (measured in arcsec per year), M the absolute magnitude and T the transverse velocity (measured in km s^{-1}). The corresponding absolute magnitude equation is very similar, $M = m + 5\log_{10}\pi + 5$, where π is the parallax. It can be seen that H 'is the magnitude a star would have when at such a distance that its proper motion appeared to be 0.1 arcsec' (Luyten 1922).

The big advantage of using H is that it is an intrinsic property of the star. This is because (see the second line of equation 1) H is a function of only M and T which are themselves intrinsic properties of the star. When H is plotted against colour (the RPM diagram) we have an equivalent to the HR diagram. This diagram is almost distance independent (when there is no interstellar extinction) due to the very weak dependence on distance of M (via the colour–absolute-magnitude relations) and the $5\log_{10} T$ distributions.

It should be noted that the reduced proper motion only uses the total proper motion and does not use any directional information. The angular part of the proper motion is dealt with separately, later on in this section, when the position of the solar apex is discussed.

Luyten (1939, 1968) used reduced proper motions to derive the local luminosity function. In these papers H was only used as a luminosity estimator and not, in conjunction with colour, as a population discriminator. More recent papers, Jones (1972a,b), Chiu (1980a,b), Reid (1984), Murray (1986) and Dawson (1986), have used the RPM diagram to identify or discriminate between various populations of stars.

In order to work out the theoretical RPM versus colour, $(O-E)$, distributions, the second line of equation (1) is used. For each population, e.g., thin old disc white dwarfs, the absolute magnitude distribution is convolved with the $5\log_{10} T$ distribution and then shifted 3.379 mag towards the bright magnitudes, i.e., smaller H. This is done as a function of $(O-E)$.

Six different populations were considered: main-sequence stars of the thin old disc (MS1), thick disc (MSint), and spheroid (MS2), red giants and subgiants of the thick disc (RGint) and spheroid (RG2) and white dwarfs of the thin old disc (WD1). Other populations, e.g., thin-disc giants, were not considered since they do not form significantly numerous populations within the HPM samples. The thick-disc populations are based on the model of Gilmore & Reid (1983, GR) and are considered since the two-component (thin old disc and spheroid) model is inadequate to explain these results.

The absolute magnitude distributions used were colour–magnitude relations, taken from various sources, with a Gaussian spread about the mean line. For the MS1, MS2, RG2 and WD1 populations, the colour–magnitude relations were the same as those used by Chiu (1980b). The sigmas used of the intrinsic Gaussian spread about these lines were similar to those in Chiu (1980b), i.e. $\sigma = 0.35$ mag for main-sequence stars, $\sigma = 0.6$ mag for giants and $\sigma = 0.8$ mag for white dwarfs. The colour–magnitude relation used for the RGint population is that for 47 Tuc (down to $M_V = 5$) and is the same as that used in the GR model. This was compiled from Cannon (1974) and Harris & Hesser (1983) with a distance modulus of 13 mag. The MSint relation is the same as that for MS2, but shifted 0.4 mag brighter.

The data for these relationships were all transformed from M_V and $(B-V)$ to M_O and $(O-E)$ using the dwarf relationships derived in Evans (1989). The error introduced by using the dwarf transforms on the data for giants is less than 0.1 in $(O-E)$. Similarly, the error in the white dwarf relationship is estimated to be less than 0.2 in $(O-E)$.

The effect of interstellar absorption is considered by using the relations $A_V = 1.6E(O-E)$ and $A_O = 1.4A_V$ (Allen 1973, p. 264). Using values for A_V taken from Burstein & Heiles (1982), it is seen that even in the largest case, the 15 Hour

Field, the reddening, $E(O-E)$, is ~ 0.1 and absorption, A_O, ~ 0.2 mag. Because this effect is so small a simplification is made in that all objects are assumed to be above the absorbing layer. This will only be incorrect for intrinsically faint objects, such as white dwarfs, and even then the effect on the positions of the theoretical RPM distributions will be small.

In order to work out the expected $5 \log_{10} T$ distribution, the parameters of the velocity ellipsoid of the population in question are needed. These are: (i) the size of the velocity dispersions along the principal axes of the ellipsoid; (ii) the directions of these axes, and (iii) the Sun's velocity with respect to this population. The details of this calculation can be found in Murray (1983) or Evans (1988).

The next important question is what values to use for the solar velocity and the ellipsoid parameters for each population? For the thin-disc population (MS1 and WD1) the basic solar motion, $U=9$, $V=11$ and $W=6$ km s^{-1} (Mihalas & Binney 1981, p. 398), is chosen, since it is the Sun's motion with respect to local neighbourhood stars, which are almost entirely from the thin disc, and is not affected by any kinematic biases. The effect on the $5 \log_{10} T$ distribution of choosing the basic solar motion instead of using, say, the standard solar motion, is a shift of ~ 0.1 mag in the peak of the distribution and is therefore not very important. The thin-disc ellipsoid parameters used were those for M0 dwarfs given in Mihalas & Binney (1981, p. 423), $\sigma_U=32$, $\sigma_V=21$ and $\sigma_W=19$ km s^{-1}. The reason for choosing the M0 values was that they were representative of late-type stars which dominate the thin-disc stars of this sample.

The data for the thick-disc population (MSint and RGint) comes mainly from Sandage & Fouts (1987), $V=42$, $\sigma_U=75$, $\sigma_V=35$ and $\sigma_W=42$ km s^{-1}. The values for U and W are assumed to be the same as that of the thin disc. It is interesting to note that Chiu (1980b) argues the case for using larger velocity dispersions for the thin disc, $\sigma=(50, 38, 33)$ km s^{-1}, as being more representative of stars at ~ 1 kpc and in order to bring the predicted and observed RPM distributions into closer agreement. Since there was no thick-disc component in this paper, it would seem reasonable that the thin-disc parameters would have to be increased in order to account for the unsuspected thick-disc population present.

The spheroid population (MS2 and RG2) data are the same as those used in Chiu (1980b), $U=15$, $V=219$, $W=15$, $\sigma_U=210$, $\sigma_V=150$ and $\sigma_W=120$ km s^{-1}. The original sources for these data are van Herk (1965) and Oort (1965).

Fig. 5 shows the $5 \log_{10} T$ distributions for the thin- and thick-disc and spheroid populations in the 8 Hour Field.

As stated earlier, the RPM diagram is almost distance independent, but this will only be true as long as both the M_O and $5 \log_{10} T$ distributions are not functions of distance themselves. As long as there are no kinematic restrictions on the data this will be the case. For the high proper motion sample considered in this paper, this will not be true. For nearby objects, the effect of a proper motion limit, $\mu_{\rm lim}$, will be small and almost all of the $5 \log_{10} T$ distributions will be included in the sample since the corresponding limiting transverse velocity, $T_{\rm lim} \propto \mu_{\rm lim} r$ (where r is distance), will be small. But for distant objects, $T_{\rm lim}$ will be large and a significant part of the $5 \log_{10} T$ distribution will be excluded. Therefore the shape of this distribution for HPM objects would be a function of distance.

Although the diagram for this sample has lost its distance independence, due to the proper motion limit, it has gained in that the H_O distributions are narrower and therefore the different populations can be separated more easily.

The effect of a proper motion limit is to exclude stars with a certain range of parameters. To calculate the effects of this we need to work out the fraction, $f(T, M)$, of stars with para-

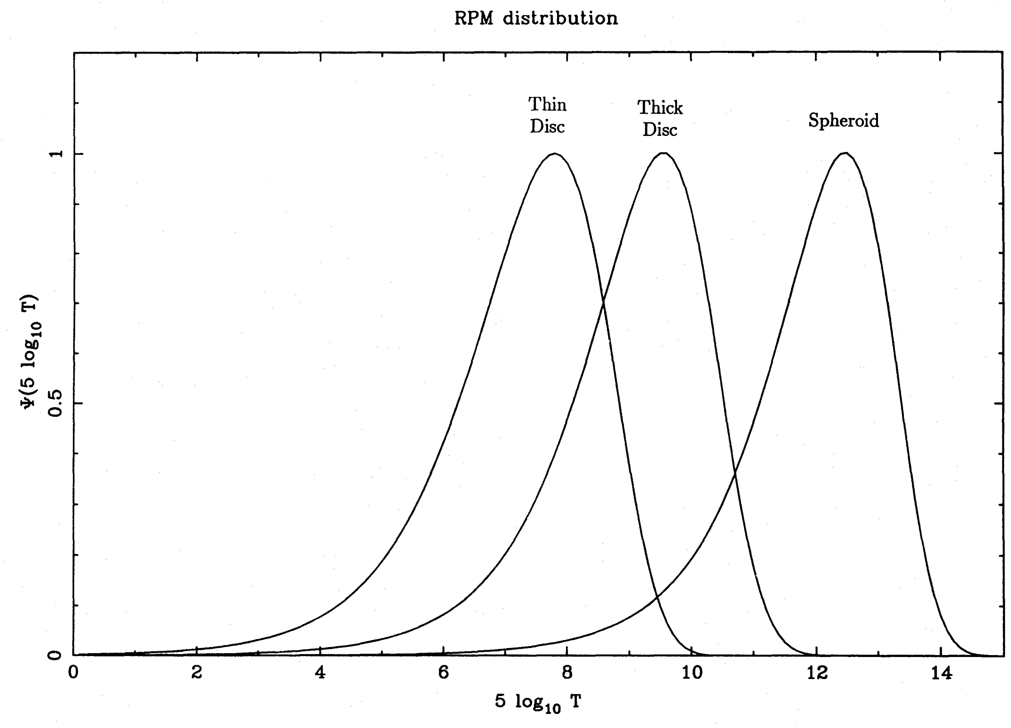

Figure 5. The $5 \log_{10} T$ distributions in the 8 Hour Field ($l=210°$, $b=35°$) for the three different kinematic populations considered. The parameters used are described in the text.

Table 7. The photometric limits for the HPM samples. The proper motion errors are also given.

	O_{lim}	E_{lim}	σ_μ (m″/y)
8 Hour Field	21.7	20.2	4.1
11 Hour Field	20.4	19.4	5.8
12 Hour Field	21.7	19.9	4.7
15 Hour Field	21.8	20.5	5.6

meters T and M that are included in the sample. This is given by the equation

$$f(T,M)=\frac{\int_0^{r_{\rm lim}(T,M)}\rho(r)\,r^2\,dr}{\int_0^{\infty}\rho(r)\,r^2\,dr}, \tag{2}$$

where $\rho(r)$ is the density law and

$$r_{\rm lim}=\min\left\{\frac{T}{4.74\mu_{\rm lim}},\ 10^{0.2(O_{\rm lim}-M_O)+1},\ 10^{0.2(E_{\rm lim}-M_E)+1}\right\}. \tag{3}$$

$O_{\rm lim}$ and $E_{\rm lim}$ are the faint photometric limits and the units for $r_{\rm lim}$, T and $\mu_{\rm lim}$ are pc, km s^{-1} and arcsec yr^{-1} respectively. The faint photometric limits used are given in Table 7. The constraints provided by the upper proper motion limits do not significantly affect the RPM distributions.

If the density law is assumed to be an exponential with scaleheight L, equation (2) simplifies to

$$f=1-e^{-x}(\tfrac{1}{2}x^2+x+1), \tag{4}$$

where $x=r_{\rm lim}/L$. For the old thin- and thick-disc populations L is calculated using scaleheights of 300 and 1000 pc respectively in the equation

$$-\frac{1}{L}=\frac{\cos l\cos b}{h_r}-\frac{\sin b}{h_z}, \tag{5}$$

where l and b are the galactic coordinates of the field and h_r and h_z are the radial scalelength and perpendicular scaleheight of the density law. The scalelength is taken to be 4.5 kpc for both populations. For the spheroid population, the density law is again assumed to be exponential and the parameters used in this case were a scaleheight of 3 kpc and a scalelength of 4.5 kpc. Although the spheroid density law is normally taken to be a de Vaucouleurs $R^{1/4}$ law [for properties of this density law see Young (1976)] an exponential law is used here as an approximation, since equation (2) would otherwise not have an easy to calculate, analytic solution. The value of 3 kpc for the scaleheight comes from the starcount fits in Sandage (1987) and is the exponential scaleheight of the spheroid density law used in this reference. To

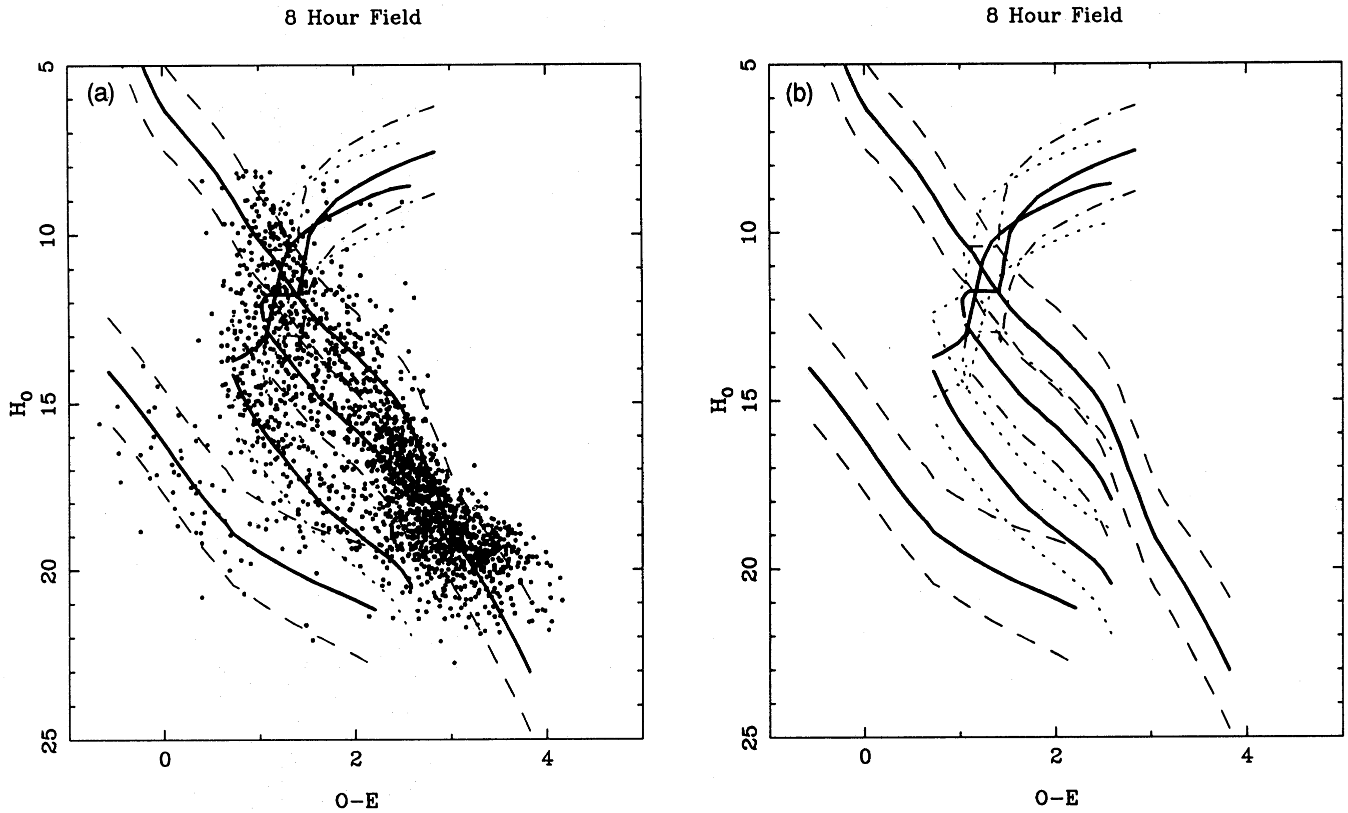

Figure 6. (a) A scatterplot of colour, $(O-E)$, versus reduced proper motion, $H_O=O+5\log_{10}\mu+5$, for the high proper motion stars in the 8 Hour Field. The predicted medians (thick lines) of the H_O distributions for six different populations are also shown. Either side of the ridge lines are drawn the 10 and 90 per cent limits of these distributions: dashed lines – thin-disc populations (main sequence and white dwarf); dot–dashed lines – thick-disc populations (main sequence and giants); dotted line – spheroid populations (main sequence and giants). (b) The same ridge lines as in (a) without the data.

see if the predicted H_O distributions were sensitive to the value of the scaleheight used, they were also calculated with a scaleheight of 4 kpc. The result was that there was very little change (<0.05 mag) in the predicted distributions, indicating that the H_O distributions for the spheroid populations are not sensitive to the detailed form of the density law assumed.

Since the predicted distributions are to be compared to observed RPMs, they must be convolved with the appropriate error functions. The error in apparent magnitude, $\sigma_O = 0.09$, can be accounted for by convolving the H_O distribution with a Gaussian of this sigma. Similarly, a colour error, $\sigma(O-E)=0.12$, needs to be added. Instead of applying this directly to the colour values it is applied to the H_O distribution via the slope, s, of the H_O versus $(O-E)$ relation, i.e. a Gaussian of half-width $\sigma = s\sigma(O-E)$ is convolved with the H_O distribution.

The predicted effects of the proper motion errors present more of a problem since a straightforward Gaussian convolution is not an accurate representation of the errors. This is because the error in $5\log_{10}\mu$ is a function of μ, which implies that to calculate the expected errors, the proper motion distribution must be calculated from the transverse velocity distribution and the density law. However, for HPM stars an approximation can be made by which a Gaussian convolution can be used to represent the proper motion errors. The details of the full error convolution, which is needed for low proper motion stars, is given in Evans (1988). Because of the high proper motion limit, the relative size of the proper motion error will always be small. Since the measuring error is 1.9μ (see Evans 1988) and the proper motion limit is 16μ, the relative proper motion error for any star in the HPM sample will always be less than 12 per cent. By taking this value to calculate the error in $5\log_{10}\mu$, $\sigma_{\log_{10}\mu} = (5\log_{10}\mathrm{e})\,\sigma_\mu/\mu$, the effects of proper motion errors are overestimated. Since $\sigma_{\log_{10}\mu} = 0.26$ mag and the half-widths of the H_O distributions are about four times larger, the overall effect of the proper motion errors on the H_O distributions will be very small (~ 3 per cent increase in width). Therefore it is not important that the proper motion errors have been overestimated. Similarly, the bias introduced by assuming a symmetric error for $5\log_{10}\mu$ will be small. A check was also carried out on the measuring error by measuring the proper motions of known quasi-stellar objects (QSOs) (assumed to be zero) in the 8 and 12 Hour Fields. The widths of these proper motion distributions confirmed the value of the measuring error. For more details see Evans (1988).

Figs 6(a) to 9(a) show the reduced proper motion diagrams for the four fields in this project, along with the expected ridge lines (medians of the H_O distributions) and the widths (10 and 90 per cent points) of the predicted distributions. Figs 6(b) to 9(b) show the ridge lines without the data, for clarity.

The general features of these RPM diagrams are: (i) a numerous population of red, $(O-E)>2$, stars; (ii) a less numerous population of bluer, $(O-E)<2$, stars, and (iii) a distinct white dwarf population.

Within the main part of the bluer stars, three populations are predicted to exist: main-sequence stars of the thin and thick discs and spheroid. Considering the widths of the two outer populations, if an intermediate population did not exist there should hardly be any stars in the central parts of these

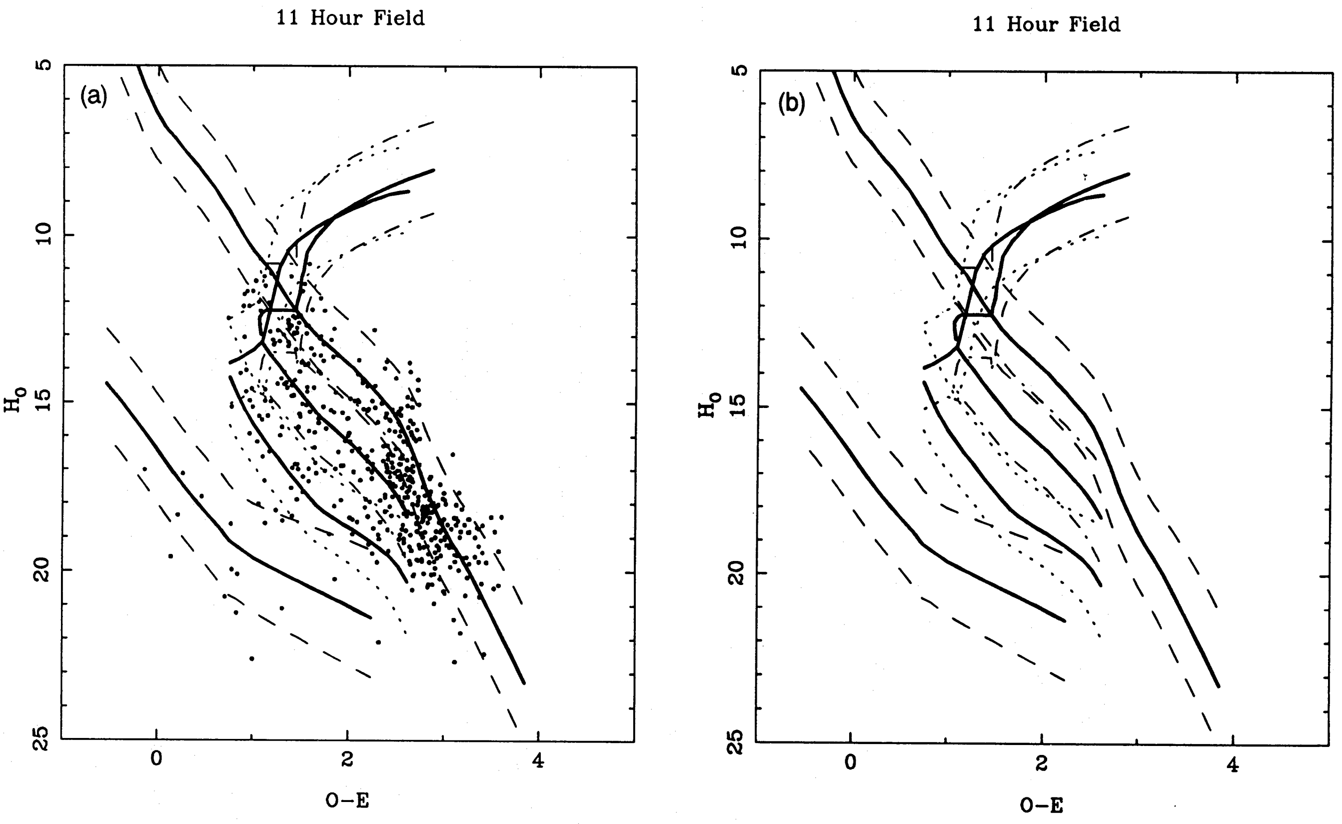

Figure 7. (a) The same as Fig. 6 but for the 11 Hour Field. (b) The 11 Hour Field ridge lines.

1992MNRAS.255..521E

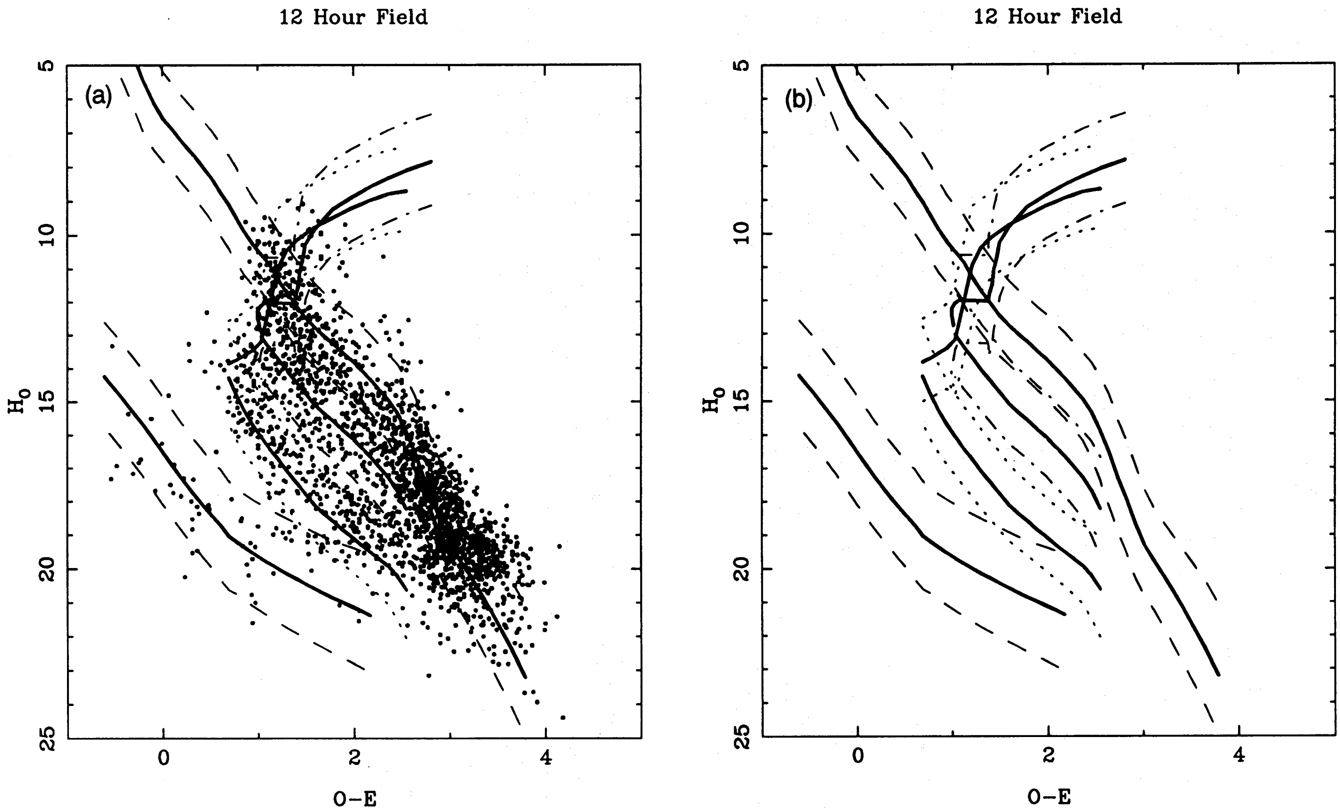

Figure 8. (a) The same as Fig. 6 but for the 12 Hour Field. (b) The 12 Hour Field ridge lines.

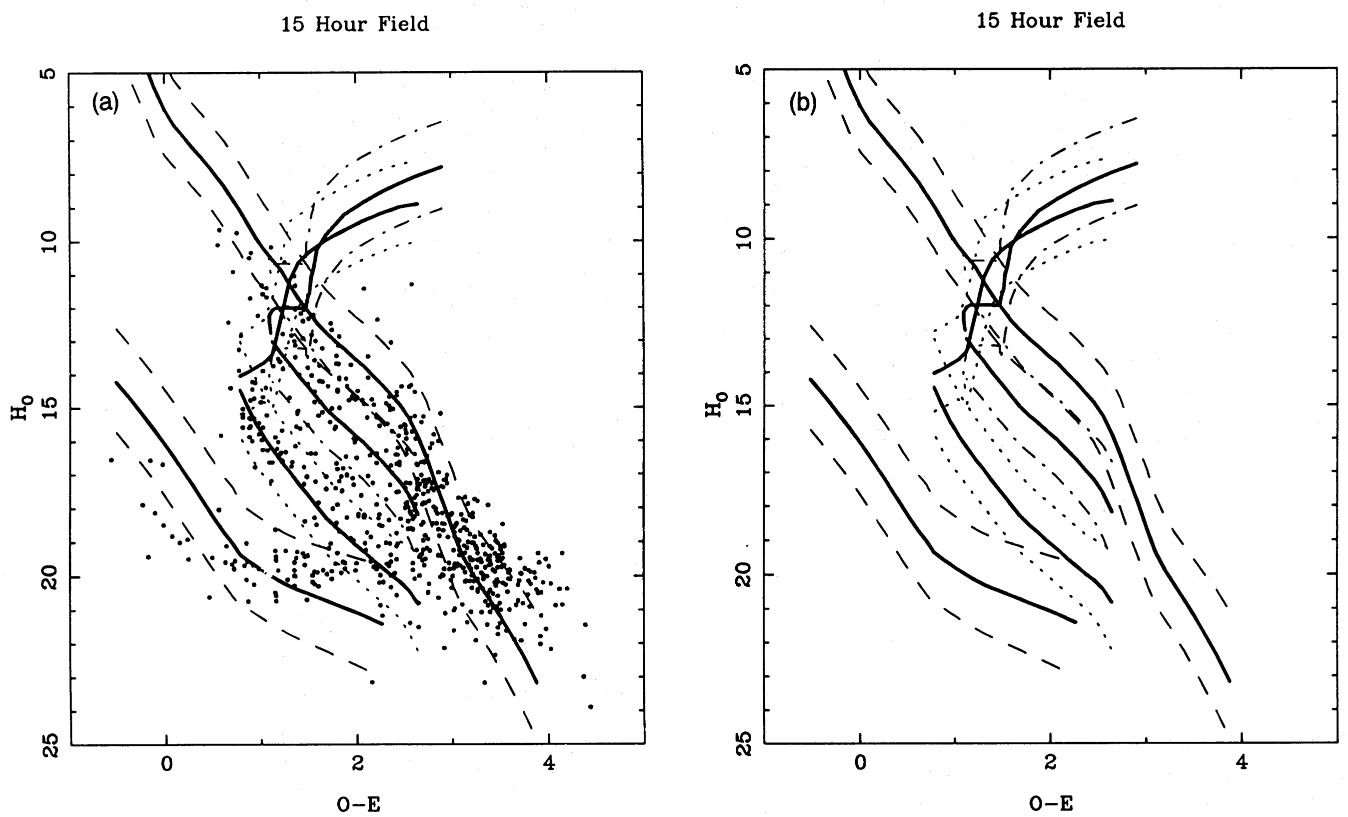

Figure 9. (a) The same as Fig. 6 but for the 15 Hour Field. (b) The 15 Hour Field ridge lines.

diagrams. The fact that there exists a very significant number of stars in this position provides further good evidence for the existence of an intermediate population and for the upgrading of the old two-component model of the Galaxy. It would be difficult to re-interpret these data in another way and still be using realistic parameters for the other populations Whether this intermediate population is a separate population or not cannot be judged from these data alone, but the simple addition of a thick-disc component seems to be a reasonable next step in the upgrade necessary to the n-component model of the Galaxy.

The giant populations are not easily observed as distinct populations in this data set, since the expected ridge lines cross over each other and the main-sequence lines. However, it is seen that the turn-offs are in good agreement with the data and in the 8 and 12 Hour Fields some distinct giant stars are seen.

The white dwarf population is very easily separated from the other populations and it is only at the red end, $(O-E)>2$, that there is any problem of identification.

4.2 The solar motion

Since the HPM samples are in four fields, relatively well spaced apart in the sky, it is possible to determine the direction of the solar motion with respect to various subsamples of the HPM sample.

The first determination of the direction of the solar motion (the solar apex) was carried out by Herschel (1783). In this paper, proper motion directions from 14 stars were used to construct great circles on the celestial sphere which crossed at the solar apex. The crossing point determined by Herschel was near the star λ Herculis ($l=50°$, $b=28°$), which is only $\sim 5°$, away from modern determinations of the solar apex position.

The method used in this paper to determine the positions of the various apices is based on the relations given in Green (1985, p. 346), which are in turn based on a method by Airy (1859). The first stage of this method is to write equations for the proper motion components, μ_α and μ_δ (note that μ_α is not the change in right ascension but the change in angular position as measured on a great circle in the direction of increasing right ascension – this yields proper motion units which are consistent with each other), in terms of the Sun's peculiar velocity with respect to this group of stars (restricted to only stars at a particular distance, d pc). By averaging the proper motions in each region of sky considered, the mean values of the peculiar motions of these stars (assumed to be randomly distributed) can be neglected, thus leaving only the secular parallactic motion.

Therefore for the ith region (containing n_i stars), we have:

$$\overline{\mu}_{\alpha i}=\frac{hX}{S_\odot}\sin\alpha_i-\frac{hY}{S_\odot}\cos\alpha_i, \tag{6}$$

$$\overline{\mu}_{\delta i}=\frac{hX}{S_\odot}\cos\alpha_i\sin\delta_i+\frac{hY}{S_\odot}\sin\alpha_i\sin\delta_i-\frac{hZ}{S_\odot}\cos\delta_i, \tag{7}$$

where $\overline{\mu}_{\alpha i}$ and $\overline{\mu}_{\delta i}$ are the mean values of the proper motions, (α_i, δ_i) are the coordinates of the region, (X, Y, Z) are the components of the Sun's peculiar velocity in the equatorial triad in km s^{-1}, $S_\odot=(\sqrt{X^2+Y^2+Z^2})$ is the total solar motion and $h(=S_\odot/4.74d)$ the secular parallax of this group of stars.

Since the number of stars in each region (for each selected group) can be quite small (50–100), it is not advisable to split the samples further into distance bins. To account for this we lose the information contained in the magnitude of the proper motions, i.e. instead of $\overline{\mu}_\alpha$ we use $\overline{\sin\theta}$, where θ is the proper motion direction. Similarly $\overline{\cos\theta}$ is used instead of $\overline{\mu}_\delta$. Since all proper motions have been normalized to unit magnitude, no distance information can be obtained from the data. However, this does have the advantage of dealing with any bias introduced by the proper motion limit.

Using the modified version of equations (6) and (7) for each of the four fields, eight equations are obtained for the three unknown quantities $hX/S_\odot$, $hY/S_\odot$, $hZ/S_\odot$, which can be calculated using the method of least squares. Note, again, that the magnitude of these quantities has no meaning, due to the normalizing of the proper motion. For deriving the position of the solar apex, only the ratios are important.

A sample of red $[(O-E)>2.3]$ stars was first selected and the apex position calculated to be $(l, b)=(63°, 14°)$ (see also Table 8 and Fig. 11). This lies approximately midway between the expected apex for the thin old disc and those for the spheroid and thick-disc populations. This indicates that in using a simple colour selection criterion, it is probable that a mixture of populations is obtained. This result is very similar in nature to that found in Luyten (1966) and Hanson (1987).

In Luyten (1966), when the apex was calculated as a function of proper motion it was found that as the proper motion increased, the position of the apex moved in a line from the expected thin-disc apex towards those of the lower metallicity populations. This is a consequence of the spheroid and thick-disc populations having higher velocities (and therefore proper motions) than the thin-disc population. As higher proper motions are sampled, the proportion of the higher velocity populations is increased, thus causing the effect observed (see Fig. 11 for the positions of these apices). In Hanson (1987), the apex was measured as a function of galactic latitude. In this case, as the latitude increased the apex moved towards the higher velocity apices. The reason for this is that the thin disc has a flatter spatial distribution than those of the spheroid or thick disc and therefore the number of thin-disc stars seen decreases more rapidly as galactic latitude increases than for the other two populations. This increases the proportion of these populations in the polar samples, causing the observed effect.

In order to minimize the effects of contamination when calculating the position of the apex, various samples were selected using the RPM diagram. Fig. 10 shows these diagrams and the selection polygons used for each of the populations selected from the four fields. The four populations selected were: (i) thin-disc red $[(O-E)>2.3]$ dwarfs; (ii) thick-disc dwarfs; (iii) spheroid dwarfs, and (iv) white dwarfs. Naturally, some of these samples are not intended to be complete, but as contamination-free as is possible.

The positions of these apices are given in Table 8 and plotted in Fig. 11. The errors for these points have been calculated using Monte Carlo simulation.

The positions of the apices of the thin-disc and spheroid subsamples are in fair agreement with the expected values. The measured position of the thick-disc apex is about 2.5σ away from its expected position. Assuming a total solar

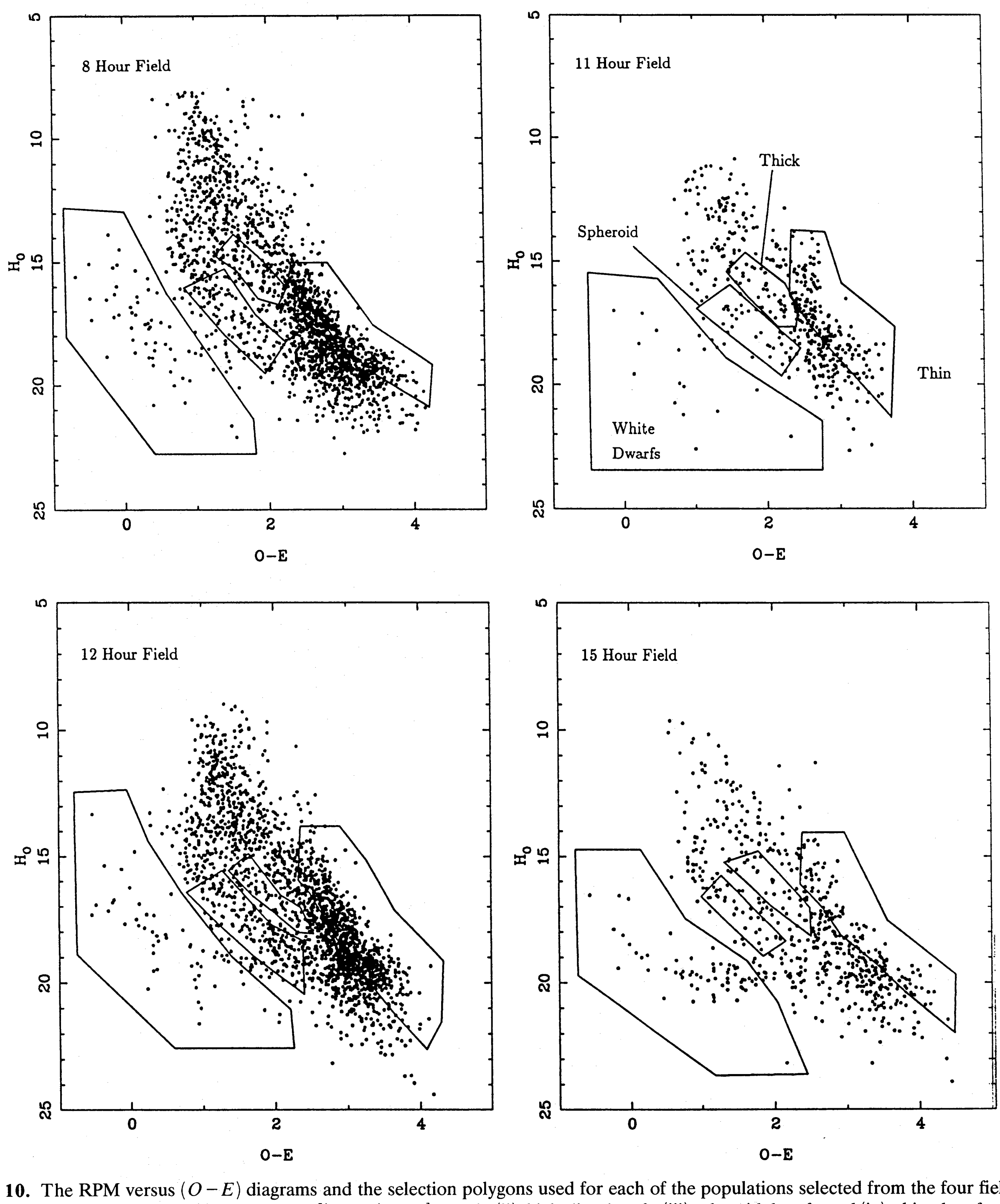

Figure 10. The RPM versus $(O-E)$ diagrams and the selection polygons used for each of the populations selected from the four fields. The four populations selected were: (i) thin-disc red $[(O-E)>2.3]$ dwarfs; (ii) thick-disc dwarfs; (iii) spheroid dwarfs, and (iv) white dwarfs.

Table 8. The position of the solar apex in terms of equatorial (α, δ) and galactic (l, b) coordinates for the various samples selected. All values are given in degrees.

	α	δ	l	b
Red dwarfs, (O–E)> 2.3	283±2	33±1	63±1	14±2
Thin disc	274±4	30±2	57±2	20±4
Thick disc	302±7	32±4	69±4	-1±5
Spheroid	312±5	53±4	92±3	6±4
White dwarfs	280±8	43±6	72±7	20±8

motion with respect to this group of stars of 43 km s^{-1} (as used earlier in this section), this apex would imply a velocity of $(U, V, W)=(15, 41, -1)$ km s^{-1}. It is only the W value that is not consistent with those given in Sandage & Fouts (1987). It is unclear what systematic effect is responsible for this discrepancy.

The position of the white dwarf apex agrees well with that given in Luyten (1980), and given its intermediate position, indicates a possible mixture of kinematic populations.

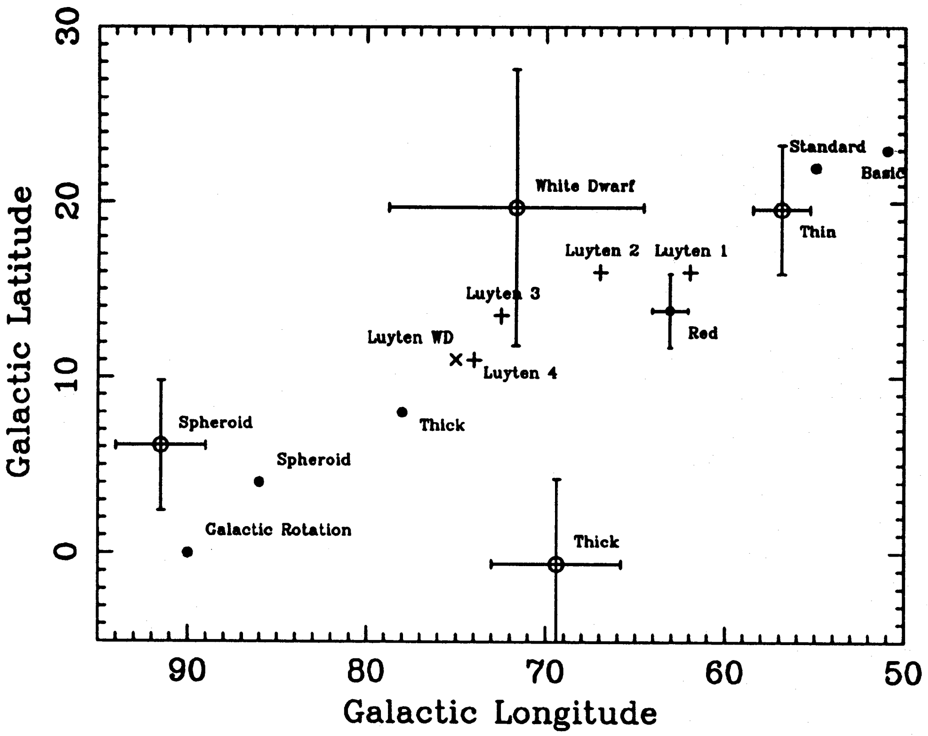

Figure 11. The derived solar apices for various subsamples of the HPM sample, along with points from various other sources. The circles (○) with error bars are the measured data points from this project. The bullets (●) are the expected values calculated from the basic and standard solar motions, and the solar velocities used earlier in this section for deriving the expected RPMs for the thick-disc and spheroid populations. The crosses (+) are taken from Luyten (1966) and have proper motion (arcsec yr^{-1}) ranges of: (i) 0.05–0.10; (ii) 0.10–0.20; (iii) 0.20–0.40, and (iv) ≥0.40. The multiplication sign (×) is from Luyten (1980) and is for white dwarfs. No errors are given by Luyten for these positions.

5 THE WHITE DWARF LUMINOSITY FUNCTION

The study of the white dwarf luminosity function (WDLF) is important since it provides information about the history of star formation in the galactic disc. The first determinations of the WDLF were by Weidermann (1967), Kovetz & Shaviv (1976) and Sion & Liebert (1977). These mainly used the white dwarf compilations of Luyten (1958) and Eggen & Greenstein (1965, 1967). The most recent determinations have been by Fleming, Liebert & Green (1986) for the hotter ($M_V \leq 13$) white dwarfs and Liebert, Dahn & Monet (1988, LDM88) for the cooler ($M_V \geq 13$) ones. The former study used stars selected from the Palomar–Green Survey (Green, Schmidt & Liebert 1986) which were first colour-selected and then spectroscopically classified, while the latter used spectroscopically confirmed white dwarfs from the LHS high proper motion catalogue.

The white dwarf sample used in this section has been selected from this project's HPM sample using the RPM and $(O-E)$ selection criteria indicated in Fig. 10. This sample was then checked by eye and any stars with dubious images or parameters were rejected. The remaining 123 white dwarfs are listed in Table 9, along with all the astrometric and photometric information available from this project.

For the white dwarfs in the 8 and 12 Hour Fields, objective prism plates exist and Fig. 12 shows the spectra of some of the brighter white dwarfs in these fields.

Comparisons of this sample with other white dwarf (WD) catalogues show that this sample is much more complete or has far deeper observational limits than previous ones. Only two WDs (LB8827 and GD173) are common to this sample and the spectroscopically confirmed WD catalogue of McCook & Sion (1987). There are no stars in this catalogue that have been missed by this project's WD sample. 10 WDs from this sample are present in the WD catalogues of Luyten

Table 9. The 123 white dwarf candidates selected from reduced proper motion diagrams (see Section 5). Column 1 gives the name. Columns 2 to 7 give the position using a 1950 epoch and equinox. Columns 8 and 9 give the total proper motion in arcsec yr^{-1} and the proper motion direction measured in the usual way with north zero and east positive. Columns 10 to 12 give the photometry (O, E and I).

Name	RA (1950) dec						μ	θ	O	(O−E)	(E−I)
	h	m	s	°	′	″	″/y	°			
WD0856+200	8	56	2.5	+19	59	6	0.043	+155	19.47	0.62	
WD0844+199	8	43	42.6	+19	56	8	0.049	−153	17.23	0.32	0.02
WD0853+194	8	53	17.9	+19	24	18	0.044	−72	20.11	0.56	
LB8888	8	52	40.2	+19	16	10	0.055	−108	16.62	0.15	-0.21
WD0850+193	8	49	35.6	+19	15	27	0.063	−175	19.85	-0.25	
WD0846+192	8	45	54.8	+19	12	10	0.037	−105	18.65	-0.48	
LB8820	8	50	28.5	+19	5	11	0.063	+127	17.62	0.18	
LB8842	8	51	23.5	+19	4	53	0.042	−161	18.00	0.33	
WD0904+191	9	3	34.8	+19	3	9	0.169	+114	20.94	1.55	
WD0850+190	8	50	4.9	+19	1	40	0.137	−126	18.22	0.38	
WD0902+190	9	2	0.4	+19	0	1	0.039	−104	17.15	-0.10	
WD0852+187	8	52	29.9	+18	44	56	0.042	−128	18.92	0.10	

Table 9 – *continued*

Name	RA (1950) h m s	dec ° ′ ″	μ ″/y	θ °	O	(O–E)	(E–I)
WD0843+187	8 43 11.3	+18 41 48	0.049	−110	18.09	-0.25	
LB8684	8 44 58.8	+18 41 30	0.151	−162	17.37	0.42	0.04
WD0846+186	8 46 14.8	+18 38 48	0.135	−169	19.36	0.68	
WD0853+186	8 53 19.4	+18 35 24	0.105	−90	19.60	0.80	
WD0858+185	8 57 40.2	+18 31 31	0.038	−131	17.29	-0.16	
WD0852+184	8 51 51.1	+18 25 42	0.041	+134	19.42	0.32	
WD0855+183	8 55 0.0	+18 19 44	0.052	+149	17.66	0.45	0.29
WD0847+183	8 47 16.9	+18 16 48	0.047	+170	19.16	0.28	
WD0848+182	8 48 11.5	+18 14 56	0.040	−117	18.38	0.17	
WD0856+181	8 55 57.7	+18 4 27	0.041	−126	20.52	0.41	
WD0845+177	8 44 43.0	+17 39 27	0.073	+152	18.84	0.11	
WD0848+176	8 47 58.4	+17 37 19	0.084	−115	14.86	-0.07	0.05
LB8999	8 55 50.2	+17 13 32	0.051	+147	18.31	0.08	
WD0856+170	8 55 54.5	+17 2 53	0.061	+172	19.61	0.63	
WD0850+169	8 50 19.8	+16 56 55	0.070	−138	19.66	0.33	
WD0903+169	9 2 55.8	+16 54 18	0.060	−175	18.46	0.37	
WD0853+169	8 52 35.7	+16 52 30	0.036	−122	18.55	-0.14	
WD0902+168	9 2 5.7	+16 49 56	0.061	+137	18.22	0.15	
WD0859+166	8 58 48.5	+16 38 57	0.040	−166	17.06	-0.49	
LP426–57	9 3 8.7	+16 37 24	0.185	−147	20.30	1.48	
WD0902+166	9 1 44.3	+16 36 25	0.035	−149	19.73	0.50	
WD0845+165	8 44 38.9	+16 31 31	0.061	+146	18.73	0.09	
LB8827	8 53 31.3	+16 22 39	0.046	−140	15.56	-0.22	-0.20
WD0845+162	8 44 43.2	+16 9 59	0.057	−172	18.57	-0.46	
WD0900+161	9 0 17.9	+16 6 15	0.039	−179	20.33	0.29	
WD0859+161	8 58 46.6	+16 3 31	0.111	−53	15.76	-0.11	-0.17
WD0858+159	8 58 5.7	+15 55 34	0.036	+1	20.85	0.89	
WD0848+159	8 48 12.7	+15 54 21	0.072	−159	19.43	0.98	
WD0853+159	8 52 41.7	+15 52 46	0.037	−154	19.77	0.35	
WD0846+158	8 46 6.4	+15 50 44	0.059	−104	20.33	0.39	
WD0902+155	9 1 57.3	+15 31 39	0.043	+174	19.07	-0.15	
WD0850+155	8 49 34.9	+15 30 39	0.040	+7	20.79	1.06	
WD0851+154	8 51 2.0	+15 22 40	0.038	−144	17.71	-0.68	
WD0847+151	8 46 52.1	+15 6 15	0.051	−98	19.16	0.33	
WD0851+151	8 50 46.2	+15 5 33	0.042	−136	19.02	-0.08	
WD1116−182	11 16 21.6	−18 14 20	0.097	−66	20.02	0.78	
WD1112−187	11 12 10.0	−18 42 53	0.063	−76	18.14	0.26	
LP792–5	11 11 27.4	−18 47 33	0.242	−60	19.18	1.31	
WD1120−188	11 19 48.6	−18 49 20	0.049	−82	19.58	1.06	
WD1117−191	11 16 57.0	−19 6 17	0.174	−31	19.55	0.71	
WD1111−193	11 10 30.6	−19 19 15	0.377	−6	19.71	1.00	
WD1120−195	11 19 52.1	−19 27 33	0.066	−44	18.72	0.46	
WD1107−196	11 7 29.4	−19 33 25	0.149	−45	18.72	0.14	
WD1115−196	11 14 52.1	−19 34 34	0.070	+107	19.39	0.77	
WD1109−199	11 9 12.0	−19 53 18	0.154	−83	16.08	-0.14	
WD1122−203	11 22 11.7	−20 15 32	0.052	−98	19.99	1.13	
WD1106−208	11 5 56.2	−20 46 59	0.165	−111	19.01	0.84	
WD1107−211	11 6 43.3	−21 7 12	0.467	−143	18.74	2.32	
WD1200+142	11 59 37.1	+14 9 48	0.114	−115	19.25	0.31	
WD1210+141	12 9 59.0	+14 6 13	0.045	+176	19.60	0.19	
WD1210+141	12 10 1.2	+14 3 6	0.063	−103	14.31	-0.53	-0.20
WD1206+139	12 5 52.5	+13 51 2	0.069	+139	17.06	-0.01	-0.22
WD1201+138	12 1 15.0	+13 47 17	0.054	+153	18.68	0.32	
WD1208+137	12 8 27.4	+13 43 16	0.042	−149	20.40	0.83	
WD1213+136	12 12 53.6	+13 33 33	0.043	+68	20.64	1.19	
WD1158+134	11 58 14.7	+13 24 23	0.055	−164	19.45	0.36	
WD1154+134	11 54 8.1	+13 22 46	0.045	+73	20.31	0.82	
LP494–12	11 56 59.8	+13 17 12	0.152	−81	18.44	0.97	-0.07
WD1157+129	11 56 41.8	+12 56 14	0.049	+176	18.05	0.56	1.33
WD1153+128	11 53 6.3	+12 49 19	0.047	−171	20.60	1.16	
WD1204+125	12 3 55.6	+12 32 54	0.100	−103	20.19	0.90	
WD1210+125	12 9 44.6	+12 30 13	0.075	−90	17.52	0.12	-0.02
WD1216+124	12 15 46.1	+12 25 21	0.074	−79	19.47	0.31	
WD1156+122	11 56 3.9	+12 9 48	0.042	−80	18.83	-0.48	
LP494–14	11 57 44.6	+12 3 39	0.206	−145	19.67	2.06	0.67
WD1208+119	12 7 34.5	+11 53 17	0.090	−95	19.69	0.36	
WD1201+117	12 0 46.7	+11 42 0	0.042	+89	19.21	-0.54	
WD1202+113	12 2 15.4	+11 18 40	0.051	−97	19.56	0.48	1.29
WD1212+112	12 12 23.2	+11 10 29	0.043	−179	20.72	1.33	
WD1204+111	12 4 4.1	+11 6 30	0.080	−116	20.34	0.88	
WD1214+110	12 14 10.4	+11 1 5	0.060	−72	19.63	0.31	
WD1159+110	11 58 50.5	+11 0 19	0.040	−150	20.92	1.26	
WD1214+106	12 13 43.8	+10 35 39	0.105	−114	19.60	0.94	
WD1207+103	12 7 29.0	+10 16 21	0.079	−138	18.01	0.08	-0.29
WD1207+102	12 7 18.7	+10 10 57	0.070	+147	18.71	0.72	0.06
WD1203+102	12 3 15.2	+10 9 39	0.041	−122	17.46	-0.12	-0.46
WD1207+099	12 6 34.0	+9 56 38	0.200	−112	19.49	0.97	
WD1204+098	12 3 30.8	+9 47 4	0.043	−91	18.66	-0.25	
WD1204+098	12 4 20.3	+9 46 18	0.043	+140	20.05	0.49	
WD1204+097	12 4 10.7	+9 43 20	0.040	+79	19.98	0.30	
WD1212+097	12 12 16.3	+9 42 38	0.047	+115	18.96	0.22	
WD1209+097	12 8 41.7	+9 41 44	0.043	−169	20.60	1.00	
WD1158+097	11 58 8.5	+9 39 55	0.044	−38	20.13	0.38	
WD1208+095	12 8 29.5	+9 30 14	0.063	−176	20.23	0.92	
WD1212+094	12 12 27.1	+9 26 45	0.040	−68	21.14	1.35	
WD1206+094	12 6 11.3	+9 22 12	0.040	+122	19.16	-0.31	
WD1208+094	12 7 30.0	+9 21 1	0.114	−102	19.96	0.23	
WD1155+092	11 54 38.3	+9 11 44	0.180	+118	18.06	0.84	0.30
WD1210+092	12 10 2.4	+9 11 32	0.041	+153	18.67	-0.23	
WD1204+092	12 4 22.3	+9 11 1	0.109	−108	17.49	-0.08	-0.27
WD1215+088	12 14 32.7	+8 50 56	0.046	−162	20.79	1.29	
WD1201+088	12 0 51.0	+8 50 47	0.200	−64	18.62	1.16	-0.38
WD1215+087	12 15 2.4	+8 44 50	0.058	−98	16.56	-0.36	
WD1200+087	11 59 38.5	+8 39 29	0.086	−122	18.06	0.11	-0.27
WD1202+086	12 1 31.4	+8 35 53	0.055	−163	16.10	0.06	0.76
WD1504+021	15 3 58.0	+2 3 26	0.087	0	19.79	0.24	
WD1455+019	14 55 22.4	+1 54 17	0.048	−99	20.43	0.07	
WD1453+019	14 52 51.4	+1 53 49	0.140	−61	19.37	0.85	
LP621–58	14 59 59.2	+1 22 41	0.234	−153	18.76	0.46	0.57
WD1454+014	14 54 12.3	+1 22 22	0.047	−123	19.74	-0.11	
WD1453+012	14 53 2.8	+1 14 57	0.071	−151	19.66	0.23	
WD1501+008	15 1 16.7	+0 46 59	0.122	+158	19.80	0.93	
GD173	14 51 17.6	+0 37 45	0.178	−100	15.32	-0.16	-0.02
WD1500+006	15 0 21.3	+0 37 7	0.056	−121	20.37	0.64	
WD1458+006	14 57 30.8	+0 36 17	0.127	−137	18.91	-0.18	
WD1451−004	14 51 1.4	−0 24 1	0.047	−129	20.11	-0.02	
WD1457−005	14 57 12.8	−0 27 57	0.071	−173	18.63	-0.24	
WD1501−005	15 1 8.6	−0 32 1	0.052	−115	20.03	1.15	
WD1452−010	14 52 1.6	−0 59 43	0.075	−82	17.32	-0.03	-0.28
WD1455−010	14 54 44.3	−1 1 3	0.054	−162	20.35	0.15	
WD1504−016	15 4 24.9	−1 36 7	0.051	−170	18.01	-0.57	

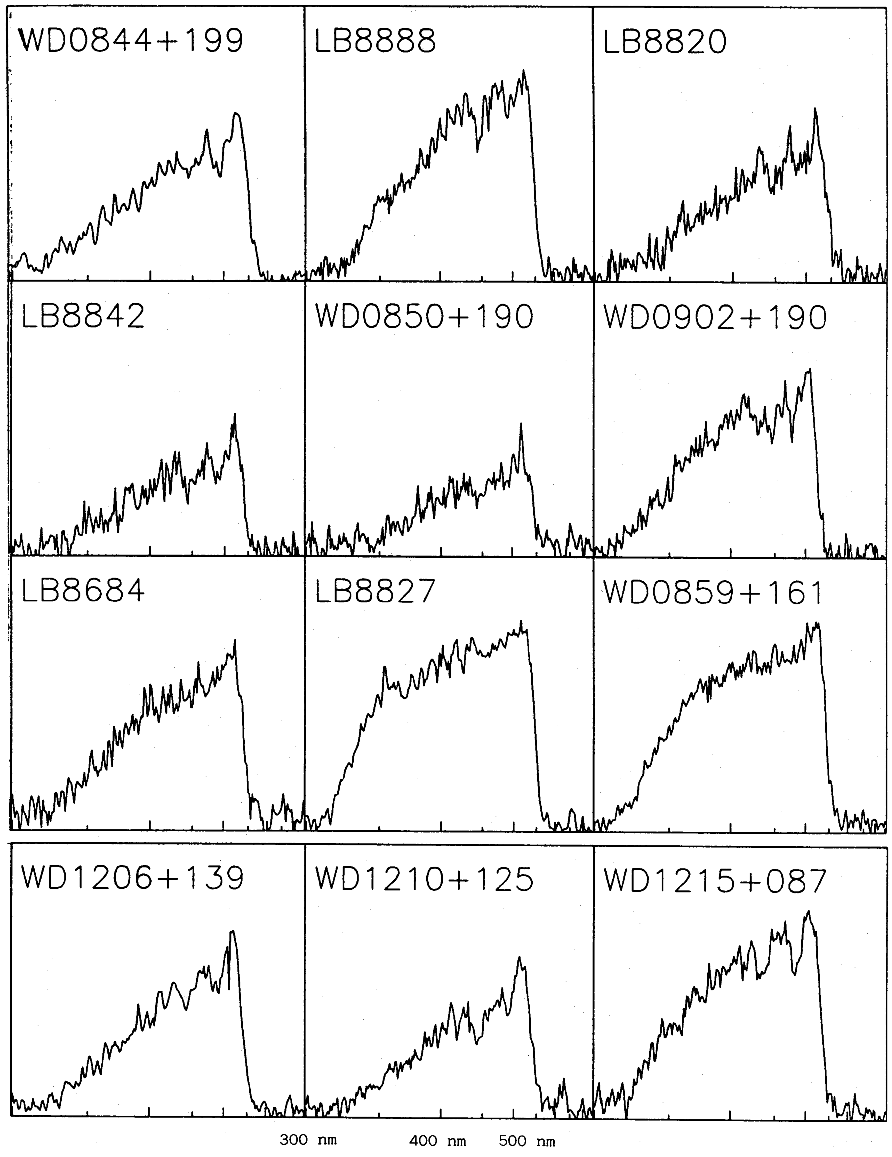

Figure 12. Objective prism spectra of some of the brighter white dwarfs in the 8 and 12 Hour Fields. The plates used were taken on the UK Schmidt Telescope and were UJ4066P and UJ4087P for the 8 and 12 Hour Fields, respectively.

(1970, 1977). In this case 13 stars from Luyten's lists are missing from this project's sample, but it is quite possible that the majority of these missed stars are not genuine white dwarfs since, as pointed out in Luyten (1977), the success rate of the catalogue decreases as the colour gets redder, and by colour class k 'probably no more than forty percent of the stars ... will prove to be genuine yellow degenerates'.

The method used to calculate the WDLF is the $1/V_{\rm max}$ method of Schmidt (1975). Using this technique, kinematic bias, introduced by the proper motion limit, is automatically corrected. In this method, stars do not make equal contributions to the space density. Instead, their contributions are weighted as the inverse of the maximum volume ($V_{\rm max}$) that a star could occupy and still be observable given the photometric and proper motion limits of the data set. This method was chosen in preference to that given in Chołoniewski (1987), which is an extended version of the C method (Lynden-Bell 1971), due to its easier implementation.

In order to calculate $V_{\rm max}$ we need a value for $d_{\rm max}$, the maximum distance that a particular star could be observed. This is given by

$$d_{\rm max} = \min\{d_{\rm obs}\mu_{\rm obs}/\mu_{\rm lim},\ d_{\rm obs}10^{0.2(O_{\rm lim}-O_{\rm obs})},\ d_{\rm obs}10^{0.2(E_{\rm lim}-E_{\rm obs})}\}, \tag{8}$$

where $\mu_{\rm lim}$, $O_{\rm lim}$, $E_{\rm lim}$ are the lower proper motion limits (see Table 2) and the faint photometric limits (see Table 7) of the data set and $d_{\rm obs}$, $\mu_{\rm obs}$, $E_{\rm obs}$ are the observed values of distance, total proper motion and O and E photometry. The value for distance, $d_{\rm obs}$, is calculated using the colour transformations given in Evans (1989) and the $(B-V)$-to-M_V relations (for DA stars) given in Sion & Liebert (1977).

For each star, a different value of $d_{\rm max}$ and a corresponding $V_{\rm max}$ ($=\Omega d^3_{\rm max}/3$, where Ω is the solid angle of the field) are calculated for each field for which the star would fall within the observational limits of that field. These values of $V_{\rm max}$ are added and then inverted to give that star's individual contri-

Table 10. The white dwarf luminosity function calculated from the HPM sample.

M_V	$\log \phi$ ($pc^{-3}M_V^{-1}$)	Errors	n
8.0	—	—	0
9.0	-4.58	(+0.27, -0.92)	4
10.0	-3.98	(+0.24, -0.60)	12
11.0	-3.52	(+0.14, -0.21)	21
12.0	-3.30	(+0.13, -0.19)	29
13.0	-3.27	(+0.14, -0.22)	17
14.0	-2.91	(+0.09, -0.12)	26
15.0	-2.86	(+0.13, -0.18)	13
16.0	-2.41	(+0.30, -∞)	1
17.0	—	—	0

bution to the luminosity function (binned by absolute magnitude). This procedure effectively combines the four fields into one field, while taking into account the different observational limits of the separate fields. The errors are calculated by taking the error contribution of each star to be equal to its $1/V_{max}$ value and then summing the errors in the usual way to obtain the errors in the luminosity function. This is the same approach that was adopted in LDM88.

This method, so far, assumes a uniform distribution of white dwarfs. In Fleming *et al.* (1986) the correction to allow for a scaleheight in the distribution of white dwarfs was introduced by defining $dV' = \exp(-z/z_0)\,dV$, where z_0 was the scaleheight. Each star's contribution would then be $1/V'_{max}$. This is effectively using a density-weighted volume, similar to that used in Section 5.5 and given by equation (5.8) of Evans (1988). The scale distances used for each field were the same as those used in the previous section for the thin disc (scaleheight 300 pc, scalelength 4.5 kpc). The effect of changing these values by ± 100 pc had little effect (<0.1 dex) on the luminosity function. The reason for this is that d_{max} was usually less than the scale distance where the correction to the volume would be small.

The resulting luminosity function for white dwarfs is given in Table 10 and shown in Fig. 13 along with the WDLF in LDM88.

Three small corrections have not been applied to the data, due to their being much smaller than the random errors. These are as given below.

(i) Systematic bias in the photometrically determined distance.

(ii) Using colour transformations appropriate for main-sequence stars on the white dwarfs. The difference is only noticeable for the hotter WDs, where the errors in the luminosity function are quite large.

(iii) Incompleteness in the HPM sample, as discussed in Section 2.

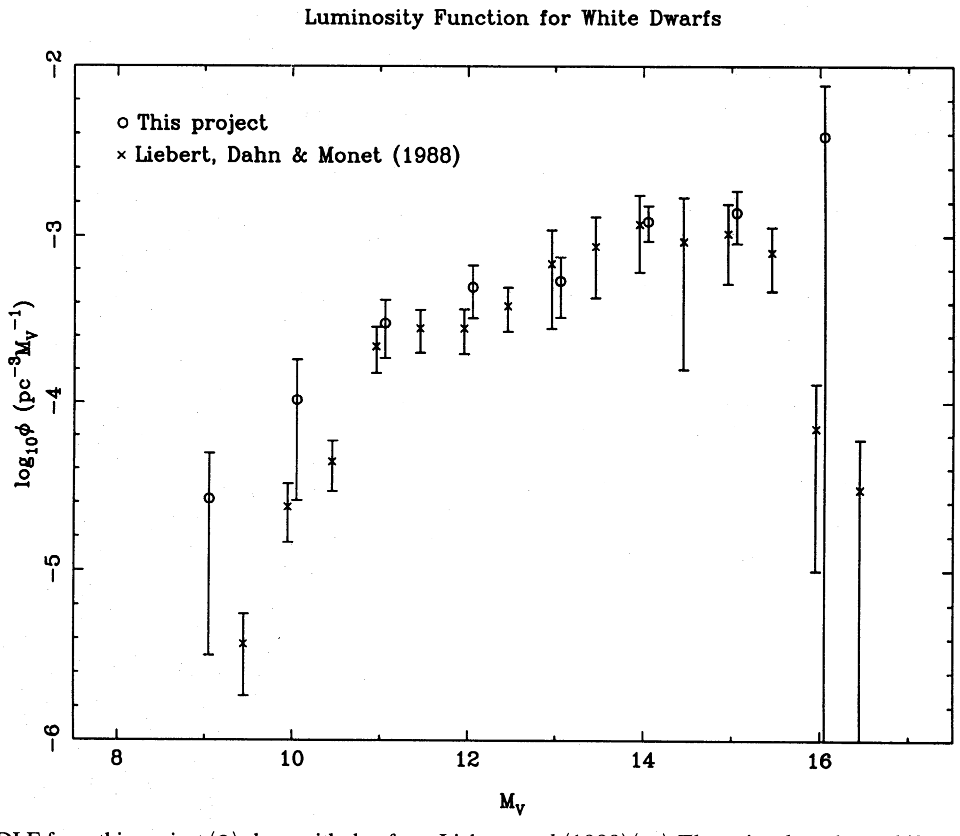

Figure 13. The WDLF from this project (○) along with that from Liebert *et al.* (1988) (×). The points have been shifted slightly in M_V so that they do not overlap. The correct absolute magnitude values are integral and half-integral.

For this data set, the random errors are far larger than the systematic ones.

As a test of the relative completeness of the sample, the average value of V/V_{max}, using the density-weighted volumes, was calculated. This was found to be 0.492 ± 0.026, agreeing well with the expected value of 0.5. Naturally, this does not imply anything about the overall completeness of the sample.

The luminosity function calculated here is in close agreement with that of LDM88 and thus adds to the strength of the conclusions of that paper. It is unfortunate that the most interesting feature of the LDM88 luminosity function, the down-turn at $M_V \sim 16$, cannot be confirmed with this sample. Due to the way that the white dwarf and spheroid RPM loci start crossing each other at about $(O-E) \sim 2$, no star could be selected using RPMs with an $(O-E)$ value much above this without needing additional classification data, e.g. spectroscopy.

ACKNOWLEDGMENTS

I thank Mike Irwin and Gerry Gilmore for useful discussions and the APM group for providing such good data. Financial support for this work was provided by SERC and Isaac Newton Studentships.

REFERENCES

Airy, G. B., 1859. *Mon. Not. R. astr. Soc.,* **19,** 175.
Allen, C. W., 1973. *Astrophysical Quantities,* 3rd edn, Athlone Press, London.
Burstein, D. & Heiles, C., 1982. *Astr. J.,* **87,** 1165.
Cannon, R. D., 1974. *Mon. Not. R. astr. Soc.,* **167,** 551.
Chiu, L.-T. G., 1980a. *Astr. J.,* **85,** 812.
Chiu, L.-T. G., 1980b. *Astrophys. J. Suppl.,* **44,** 31.
Chołoniewski, J., 1987. *Mon. Not. R. astr. Soc.,* **226,** 273.
Dawson, P. C., 1986. *Astrophys. J.,* **311,** 984.
Eggen, O. J., 1979. *Astrophys. J. Suppl.,* **39,** 89.
Eggen, O. J. & Greenstein, J. L., 1965. *Astrophys. J.,* **141,** 83.
Eggen, O. J. & Greenstein, J. L., 1967. *Astrophys. J.,* **150,** 927.
Evans, D. W., 1988. *PhD thesis,* Cambridge University.
Evans, D. W., 1989. *Astr. Astrophys. Suppl.,* **78,** 249.
Fleming, T. A., Liebert, J. & Green, R. F., 1986. *Astrophys. J.,* **308,** 176.
Giclas, H. L., Burnham, R. & Thomas, N. G., 1971. *Lowell Proper Motion Survey,* Lowell Observatory, Flagstaff, Arizona.
Gilmore, G. & Reid, N., 1983. *Mon. Not. R. astr. Soc.,* **202,** 1025 (GR).
Gliese, W. & Jahreiß, H., 1980. *Astr. Astrophys.,* **85,** 350.
Green, R. F., Schmidt, M. & Liebert, J., 1986. *Astrophys. J. Suppl.,* **61,** 305.
Green, R. M., 1985. *Spherical Astronomy,* Cambridge University Press, Cambridge.
Hanson, R. B., 1987. *Astr. J.,* **94,** 409.
Harris, W. E. & Hesser, J. E., 1983. *Astrophys. J. Lett.,* **268,** L111.
Herschel, W., 1783. *Phil. Trans.,* **73,** 247.
Jones, E. M., 1972a. *Astrophys. J.,* **173,** 671.
Jones, E. M., 1972b. *Astrophys. J.,* **177,** 245.
Kovetz, A. & Shaviv, G., 1976. *Astr. Astrophys.,* **52,** 403.
Kron, G. E., Gascoigne, S. C. B. & White, H. S., 1957. *Astr. J.,* **62,** 605.
La Bonte, A. E., 1970. *Proper Motions, IAU Colloq. No. 7,* p. 26, ed. Luyten, W. J., University of Minnesota, Minneapolis.
Liebert, J., Dahn, C. C. & Monet, D. G., 1988. *Astrophys. J.,* **332,** 891 (LDM88).
Luyten, W. J., 1922. *Lick Obs. Bull.,* No. 336.
Luyten, W. J., 1939. *Univ. Minn. Obs. Publ.,* **2,** 123.
Luyten, W. J., 1955. *A Catalogue of 1849 Stars with Proper Motions Exceeding 0″.5 Annually,* Lund Press, Minneapolis, Minnesota.
Luyten, W. J., 1957. *A Catalogue of 9867 Stars in the Southern Hemisphere with Proper Motions Exceeding 0″.2 Annually,* Lund Press, Minneapolis, Minnesota.
Luyten, W. J., 1958. *On the Frequency of White Dwarfs in Space,* The Observatory of the University of Minnesota, Minneapolis.
Luyten, W. J., 1961. *A Catalogue of 7127 Stars in the Northern Hemisphere with Proper Motions Exceeding 0″.2 Annually,* Lund Press, Minneapolis, Minnesota.
Luyten, W. J., 1962. *First Supplement to the LTT Catalogues,* The Observatory of the University of Minnesota, Minneapolis.
Luyten, W. J., 1966. *Proper Motion Survey with the 48-inch Schmidt Telescope,* **X,** University of Minnesota Press, Minneapolis.
Luyten, W. J., 1968. *Mon. Not. R. astr. Soc.,* **139,** 221.
Luyten, W. J., 1970. *White Dwarfs,* University of Minnesota Press, Minneapolis.
Luyten, W. J., 1977. *White Dwarfs II,* University of Minnesota Press, Minneapolis.
Luyten, W. J., 1979. *NLTT Catalog,* University of Minnesota Press, Minneapolis.
Luyten, W. J., 1980. *Proper Motion Survey with the 48-inch Schmidt Telescope,* **LIV,**University of Minnesota Press, Minneapolis.
Lynden-Bell, D., 1971. *Mon. Not. R. astr. Soc.,* **155,** 95.
McCook, G. P. & Sion, E. M., 1987. *Astrophys. J. Suppl.,* **65,** 603.
Mihalas, D. & Binney, J., 1981. *Galactic Astronomy,* W. H. Freeman & Co., San Francisco.
Murray, C. A., 1983. *Vectorial Astrometry,* Adam Hilger, Bristol.
Murray, C. A., 1986. *Mon. Not. R. astr. Soc.,* **223,** 649.
Newcomb, J. S., 1975. In: *Image Processing Techniques in Astronomy,* p. 159, eds de Jager, C. & Nieuwenhuijzen, H., Reidel, Dordrecht, Holland.
Oort, J. H., 1965. In: *Galactic Structure (Stars and Stellar Systems),* Vol. 5, p. 455, eds Blaauw, A. & Schmidt, M., University of Chicago Press, Chicago.
Porter, J. G., 1892. *Astr. J.,* **12,** 25.
Reid, N., 1984. *Mon. Not. R. astr. Soc.,* **206,** 1.
Sandage, A., 1987. *Astr. J.,* **93,** 610.
Sandage, A. & Fouts, G., 1987. *Astr. J.,* **92,** 74.
Schmidt, M., 1975. *Astrophys. J.,* **202,** 22.
Sion, E. M. & Liebert, J., 1977. *Astrophys. J.,* **213,** 468.
van Herk, G., 1965. *Bull. astr. Insts Neth.,* **18,** 71.
van Maanen, A., 1915. *Astrophys. J.,* **41,** 187.
Weidemann, V., 1967. *Zeitschrift für Astrophysik,* **67,** 286.
Young, P. J., 1976. *Astr. J.,* **81,** 807.